Impacts of inverse magnetic catalysis on screening masses of neutral pions and sigma mesons in hot and magnetized quark matter

Bing-kai Sheng
Center for theoretical physics and College of Physics, Jilin University, Changchun 130012, People's Republic of China
and School of Fundamental Physics and Mathematical Sciences, Hangzhou Institute for Advanced Study, UCAS, Hangzhou, 310024, China

Xinyang Wang*
Department of Physics, Jiangsu University, Zhenjiang 212013, People's Republic of China

Lang Yu†
Center for theoretical physics and College of Physics, Jilin University, Changchun 130012, People's Republic of China

(Received 28 October 2021; accepted 18 January 2022; published 1 February 2022)

We investigate the screening masses of neutral pions and sigma mesons in hot and magnetized quark matter in the framework of a two-flavor lattice-improved Nambu–Jona-Lasinio (NJL) model with a magnetic-field-dependent coupling constant, which is determined by utilizing the results from lattice QCD simulations. Since such a model can well reproduce inverse magnetic catalysis (IMC), by comparing with the standard NJL model, we systemically analyze the impacts of IMC on the temperature and magnetic field dependences of the longitudinal and transverse screening masses of the chiral partners, i.e., π^0 and σ mesons, as well as the screening mass differences between them. Particularly, it is found that the eB dependences of two alternative (pseudo)critical temperatures for the chiral transition defined by $\sigma - \pi^0$ meson screening mass differences are consistent with that defined by the quark condensate.

DOI: 10.1103/PhysRevD.105.034003

I. INTRODUCTION

The properties of strong interactions, which are described by the theory of quantum chromodynamics (QCD), in the presence of external magnetic fields have been extensively investigated in the past years (see, e.g., Refs. [1–3] for recent reviews). This is because of strong magnetic fields that are expected to exist in the early Universe [4,5], compact stars like magnetars [6], and the noncentral relativistic heavy ion collisions at RHIC and LHC [7–10]. In these physical situations, the magnitude of the magnetic fields, ranging from m_π^2 to multiples of m_π^2, could be comparable with strong interactions ($eB \gtrsim \Lambda_{\mathrm{QCD}}^2$), so that the properties of strongly interacting matter will be significantly modified by such strong magnetic fields. Particularly, there are a variety of new and intriguing phenomena induced by the interplay between magnetic fields and nonperturbative properties of QCD, for instance, chiral magnetic effect [11–13], magnetic catalysis (MC) [14–17], inverse magnetic catalysis (IMC) [18,19], and vacuum superconductivity [20,21], and so on. Thus, a deep and comprehensive theoretical understanding of QCD phase structure under a background magnetic field is desired.

One of the important aspects of the QCD phase diagram is the chiral symmetry breaking and restoration. It is well known that the chiral condensate is the order parameter of the chiral phase transition in the chiral limit. And, for physical quark masses, this transition is changed from the second-order one to the crossover at zero baryon density, revealed by Refs. [22,23], but the chiral condensate can still act as an approximate order parameter to exhibit the characteristic behavior of chiral symmetry breaking and restoration. When the external magnetic field is present, early lattice studies [24–28], as well as almost all low-energy effective models and theories of QCD [14–17,29–40], showed that the chiral condensate increases as the magnetic field grows, a phenomenon called magnetic catalysis [14–17]. Correspondingly, the chiral pseudocritical temperature T_{pc} of the chiral crossover increases with the magnetic

*wangxy@ujs.edu.cn
†yulang@jlu.edu.cn

Published by the American Physical Society under the terms of the Creative Commons Attribution 4.0 International license. Further distribution of this work must maintain attribution to the author(s) and the published article's title, journal citation, and DOI. Funded by SCOAP³.

field B. However, according to recent results of the lattice simulations by employing staggered quarks with physical quark masses, it is found that at low temperatures magnetic catalysis still remains, while at the temperatures around the chiral crossover, the chiral condensate would be surprisingly decreased by the magnetic field, which is called inverse magnetic catalysis [18,19]. As a result of such an effect, $T_{\rm pc}$ is evidently reduced by the increasing of the magnetic field strength [18,19]. Since then, there have been a large number of studies [41–58] trying to explore the underlying physics behind this puzzle problem. In particular, one possible idea is that by incorporating magnetic-dependent or thermomagnetic-dependent coupling constants in the Nambu–Jona-Lasinio (NJL)-type models [46,47,51,52,55], IMC as well as the reduction of $T_{\rm pc}$ as the magnetic field grows can be reproduced to a great extent. And it might be considered as an indirect way of introducing the sea effect in the effective model descriptions, since such a contribution, qualitatively speaking, is the main physical reason for the appearance of IMC, as argued by the lattice simulations in Ref. [43].

On the other hand, the response of the properties of mesons to B will also help to explore the phase structure of QCD in an external magnetic field. For example, light mesons like pions are Nambu-Goldstone bosons corresponding to the chiral symmetry breaking, so the study on their properties is conducive to understanding the chiral phase transition under the magnetic field. Besides, for the chiral partners such as neutral pions and sigma mesons, their mass difference can be also considered as an order parameter to describe the behavior of the chiral crossover. For this reason, the pole masses of light mesons in the presence of magnetic fields have been widely evaluated in the framework of chiral perturbation theory [59], the linear sigma model [60–62], NJL model [63–77], relativistic or nonrelativistic constituent quark model [78–80], and lattice QCD (LQCD) simulations [81–89]. In addition, another important effect of the magnetic field on mesons is that charged vector mesons are conjectured to condense for sufficiently strong magnetic fields [20,21]. The existence of the charged rho condensation has been studied by a lot of work [20,21,81,82,84,87,88,90–101], and it is still an open question right now.

However, as we have mentioned in Ref. [75], unlike the pole masses, the screening masses of light mesons at finite temperature under the magnetic field were studied in only a few trials [64,65,70,75]. In fact, the screening meson masses are also useful quantities for understanding the properties of QCD, since light mesons play an important role in nuclear physics as mediators of nuclear or quark interactions and the range of force is determined by the inverse of screening mass. Especially, the screening mass difference between mesonic chiral partners is strongly related to the chiral symmetry breaking and restoration of QCD. Namely, the screening masses of them become degenerate when the chiral symmetry gets restored. Hence, the temperature dependence of meson screening masses at vanishing magnetic field has been investigated in the NJL-type models [102–106], in holography QCD [107], and in LQCD [108–111]. But when a magnetic field is applied, there were only several papers [64,65,70,75] that explored the influence of magnetic fields on the screening masses of mesons in the hot medium. Note that, in our recent work [75], we systematically presented the calculations of the screening masses for neutral pions under magnetic fields in the NJL model within full random phase approximation (RPA) and solved the limitations of the previous studies. Now we hope to extend our evaluations to the screening mass difference between neutral pions and sigma mesons in the magnetic field, in order to analyze the effects of magnetic fields on the chiral phase transition in an alternative way. Furthermore, it is found in Refs. [68,72,75] that the pole masses of neutral pions suffer a sudden jump at Mott transition temperature in the presence of an external magnetic field. This discontinuity may disturb the study for the B-dependent behavior of the chiral phase transition, whereas the temperature dependence of the screening masses for neutral pions has no jump behavior in the whole temperature range at finite magnetic field [75]. This implies that, compared with the pole masses, the screening masses of mesons may play a better role in investigating the chiral phase transition under magnetic fields.

In this work, we will concentrate on studying the impacts of IMC on the screening masses of neutral pions and sigma mesons, especially the mass difference between them, in hot and magnetized quark matter within the framework of a lattice-improved two-flavor NJL model, where IMC can be well reproduced by adopting a magnetic-dependent coupling constant [18]. In this scenario, we phenomenologically determine the magnetic field dependence of the four-fermion interaction coupling constant utilizing the magnetic-dependent constituent quark masses, which are inferred from the baryon mass spectrum as a function of the magnetic field by employing lattice simulations [55]. Moreover, it should be emphasized that we choose the proper-time regularization scheme which can guarantee the sound velocities of mesons cannot be larger than unity, according to the arguments in Ref. [75]. And an infrared cutoff $\Lambda_{\rm IR}$ is introduced by considering the color confinement so as to remove unphysical decay thresholds for sigma mesons into quarks and antiquarks [112]. Additionally, for the choice of the regularization scheme, as argued in the recent Refs. [113,114], the vacuum magnetic regularization scheme helps to avoid unphysical results for the magnetization, in contrast with the magnetic-field-independent regularization scheme. According to the arguments in Ref. [113], we can find that this is because the purely magnetic part in the former one experiences the same regularization prescription as the vacuum part. And it is not related to whether they separate the vacuum part from the purely magnetic part. Hence, our mixing up of the vacuum and magnetic parts does not lead to any inconsistencies for the magnetization.

This paper is organized as follows. In Sec. II, we will first introduce the two-flavor NJL model in the presence of an external magnetic field and show the gap equation in the mean field approximation. Next, in Sec. III, the mesonic correlation function is derived by using the RPA approach, and the analytical expressions of the polarization functions for scalar-isoscalar and pseudoscalar-isovector channels are calculated in detail by using the propagators of quarks in the magnetic field. Then, in Sec. IV, after incorporating the lattice-improved NJL model with the magnetic-dependent coupling constants, we will show the corresponding numerical results and make some discussions. Finally, the summary and conclusions will be presented in Sec. V.

II. NJL MODEL AND THE GAP EQUATION

In the presence of an external electromagnetic field, the two-flavor NJL model [115,116] reads

$$\mathcal{L}_{\rm NJL} = \bar{\psi}(i\gamma^\mu D_\mu - \hat{m})\psi + G[(\bar{\psi}\psi)^2 + (\bar{\psi}i\gamma_5\boldsymbol{\tau}\psi)^2], \tag{1}$$

where $D_\mu = \partial_\mu + i\hat{Q}eA_\mu^{\rm ext}$ is the covariant derivative which couples quarks to an external U(1) gauge field $A_\mu^{\rm ext}$, i.e., the electromagnetic field, and $\hat{Q} = {\rm diag}(Q_u, Q_d) = {\rm diag}(2/3, -1/3)$ is the quark charge matrix in the two-flavor space. The current quark mass matrix is $\hat{m} = {\rm diag}(m_u, m_d)$ and explicitly brings chiral symmetry breaking. In this paper, the current masses of up and down quarks are set to equal with each other, i.e., $m_u = m_d = m_0$, but the isospin symmetry is still broken by the external electromagnetic field. The capital G is the coupling constant corresponding to the scalar and pseudoscalar channels, and $\boldsymbol{\tau} = (\tau_1, \tau_2, \tau_3)$ are Pauli matrices in the two-flavor space. The fields of quarks are denoted by $\psi = (u, d)^T$.

The constituent quark mass m is determined by the gap equation

$$m = m_0 - 2G\langle\bar{\psi}\psi\rangle, \tag{2}$$

which is derived by using the Hartree approximation [117,118]. Here, the quark (chiral) condensate $\langle\bar{\psi}\psi\rangle$ is defined by $\langle\bar{\psi}\psi\rangle \equiv -{\rm Tr}S(x,x)$, where Tr denotes the trace of the propagator of constituent quarks, i.e., $S(x,x')$ in flavor, color, and spinor space. The propagator of constituent quarks is defined by

$$(i\gamma^\mu D_\mu - m)S(x,x') = i\delta^{(4)}(x-x'). \tag{3}$$

In this paper, we investigate the effects of an external constant magnetic field on the screening masses of the mesons and, thus, choose the Landau gauge $A_\mu^{\rm ext} = (0, 0, -Bx, 0)$ corresponding to the magnetic field $\boldsymbol{B} = (0, 0, B)$ along the positive z direction. The Lorentz symmetry is broken by the background magnetic field at zero temperature, i.e., ${\rm SO}(1,3) \to {\rm SO}(2) \otimes {\rm SO}(1,1)$. From Eq. (3), we can obtain the analytical result of the propagator of constituent quarks in Minkowski space, i.e., $g_{\mu\nu} = {\rm diag}(1, -1, -1, -1)$, and it reads

$$S(x,x') = e^{i\Phi_f(\boldsymbol{r}_\perp, \boldsymbol{r}'_\perp)}\tilde{S}(x-x'), \tag{4}$$

where $\Phi_f(\boldsymbol{r}_\perp, \boldsymbol{r}'_\perp) = \frac{Q_f eB(x+x')(y-y')}{2}$ is the so-called Schwinger phase [119] and the index f is the flavor index, i.e., $f = u, d$ and $\boldsymbol{r}_\perp = (x, y)$. The translation invariant part of the propagator $\tilde{S}(x-x')$ reads

$$\tilde{S}(x-x') = \int \frac{d^4p}{(2\pi)^4} e^{-ip\cdot(x-x')}\tilde{S}(p), \tag{5}$$

where

$$\begin{aligned}\tilde{S}(p) = \int_0^\infty ds \exp\Big\{ & is[p_0^2 - p_3^2 - m^2 + i\epsilon] - is\boldsymbol{p}_\perp^2 \\ & \times \frac{\tan(sQ_f eB)}{sQ_f eB}\Big\}[\gamma^\mu p_\mu + m + (p^1\gamma^2 - p^2\gamma^1) \\ & \times \tan(sQ_f eB)][1 - \gamma^1\gamma^2\tan(sQ_f eB)]. \end{aligned} \tag{6}$$

Here, $\boldsymbol{p}_\perp^2 = p_1^2 + p_2^2$.

The gap equation in vacuum can be expressed explicitly as follows by using the quark propagator of Eq. (4):

$$m = m_0 + 4Gm{\rm I}_{1,{\rm vac}}(m^2), \tag{7}$$

where the integral ${\rm I}_{1,{\rm vac}}(m^2)$ is defined by

$${\rm I}_{1,{\rm vac}}(m^2) \equiv \frac{N_c}{8\pi^2}\sum_{f=u,d}\int_0^\infty ds \frac{e^{-m^2 s}}{s}|Q_f eB| \times \coth(s|Q_f eB|). \tag{8}$$

At finite temperature, the rotation symmetry of spacetime is further broken by the external heat reservoir, namely, ${\rm SO}(2) \otimes {\rm SO}(1,1) \to {\rm SO}(2)$, which means that the system is merely invariant under SO(2) transformation in the plane which is vertical to the direction of the magnetic field. The sum over the Matsubara frequencies of fermions needs to be introduced to the integral of the quark momenta, i.e., $p^0 \to i\omega_l^F$, where $\omega_l^F = (2l+1)\pi T$, $l = 0, \pm1, \pm2\ldots$, and the gap equation reads

$$m = m_0 + 4Gm{\rm I}_1(m^2), \tag{9}$$

where the integral ${\rm I}_1(m^2)$ is defined as follows:

$$\mathrm{I}_1(m^2) \equiv \frac{N_c}{4\sqrt{\pi^3}} \sum_{f=u,d} \int_0^\infty ds \frac{e^{-m^2 s}}{\sqrt{s}} [T\theta_2(0, e^{-4\pi^2 T^2 s})] \times |Q_f eB| \coth(s|Q_f eB|), \tag{10}$$

and $\theta_2(u, q)$ is the Jacobi theta function [120]. Note that when the temperature T goes to zero, $\mathrm{I}_1(m^2) \to \mathrm{I}_{1,\mathrm{vac}}(m^2)$ is due to

$$\lim_{T\to 0} T\theta_2(0, e^{-4\pi^2 T^2 s}) = \frac{1}{2\sqrt{\pi s}}. \tag{11}$$

As mentioned above, we employ the proper-time regularization scheme with the ultraviolet cutoff Λ_{UV} and the infrared cutoff Λ_{IR} [112,121,122] in the model. The regularized integrals in the gap equations at zero and finite temperature read

$$\mathrm{I}^{\mathrm{PT}}_{1,\mathrm{vac}}(m^2) \equiv \frac{N_c}{8\pi^2} \sum_{f=u,d} \int_{\frac{1}{\Lambda^2_{\mathrm{UV}}}}^{\frac{1}{\Lambda^2_{\mathrm{IR}}}} ds \frac{e^{-m^2 s}}{s} |Q_f eB| \times \coth(s|Q_f eB|) \tag{12}$$

and

$$\mathrm{I}^{\mathrm{PT}}_1(m^2) \equiv \frac{N_c}{4\sqrt{\pi^3}} \sum_{f=u,d} \int_{\frac{1}{\Lambda^2_{\mathrm{UV}}}}^{\frac{1}{\Lambda^2_{\mathrm{IR}}}} ds \frac{e^{-m^2 s}}{\sqrt{s}} [T\theta_2(0, e^{-4\pi^2 T^2 s})] \times |Q_f eB| \coth(s|Q_f eB|), \tag{13}$$

respectively. Note that the gap equations at zero and finite temperature, i.e., Eqs. (7) and (9), are in Euclid space, by performing the Wick rotation $s \to -is$.

III. THE SCREENING MASSES OF NEUTRAL PION AND SIGMA MESON

We evaluate the screening masses of neutral pions and sigma mesons by following Ref. [104]. First, we consider the mesonic correlation function defined by

$$\eta_{\xi\xi}(x) \equiv \langle 0|\mathrm{T}[J_\xi(x) J^\dagger_\xi(0)]|0\rangle, \tag{14}$$

where $\xi = \pi^0$ for the neutral pion, $\xi = \sigma$ for the sigma meson, and capital T denotes the time-ordered product. Note that there is no mixing term considered here. The third component of the pseudoscalar isovector current is

$$J_{\pi^0}(x) = \bar\psi(x) i\gamma_5 \tau_3 \psi(x), \tag{15}$$

and the scalar isoscalar current is

$$J_\sigma(x) = \bar\psi(x)\psi(x) - \langle\bar\psi(x)\psi(x)\rangle. \tag{16}$$

Then, the Fourier transformation of $\eta_{\xi\xi}(x)$ reads

$$\chi_{\xi\xi}(k) = i \int d^4x e^{ik\cdot x} \langle 0|\mathrm{T}[J_\xi(x) J^\dagger_\xi(0)]|0\rangle. \tag{17}$$

The correlation function in momentum space, i.e., $\chi_{\xi\xi}(k)$, can be obtained by using the RPA method [117,118], and it is given by

$$\chi_{\xi\xi}(k) = \Pi_\xi(k) + 2G\Pi_\xi(k)\chi_{\xi\xi}(k), \tag{18}$$

where the one quark-loop polarization function $\Pi_\xi(k)$ is defined by

$$\Pi_\xi(k) \equiv -i \int \frac{d^4p}{(2\pi)^4} \mathrm{Tr}[\Gamma_\xi \tilde S(p) \Gamma_\xi \tilde S(p-k)], \tag{19}$$

and $\Gamma_{\pi^0} = i\gamma_5\tau_3$, $\Gamma_\sigma = \mathbf{1}$. Note that two Schwinger phases of the quark-antiquark pair cancel with each other in the neutral meson polarization functions. Substituting Eq. (6) into Eq. (19) and completing the tedious calculations, we obtain the explicit expressions of the polarization functions at zero temperature as follows:

$$\begin{aligned}\Pi_{\pi^0,\mathrm{vac}}(\boldsymbol{k}^2_\perp, \boldsymbol{k}^2_\parallel) = {} & \frac{N_c}{4\pi^2} \sum_{f=u,d} \int_0^\infty ds \int_0^1 du \exp\left[-m^2 s - \frac{s(1-u^2)}{4}\boldsymbol{k}^2_\parallel - \frac{\cosh(s|Q_f eB|) - \cosh(su|Q_f eB|)}{2|Q_f eB| \sinh(s|Q_f eB|)}\boldsymbol{k}^2_\perp\right] \\ & \times \left\{\left(m^2 + \frac{1}{s} - \frac{1-u^2}{4}\boldsymbol{k}^2_\parallel\right)\frac{|Q_f eB|}{\tanh(s|Q_f eB|)} - \frac{|Q_f eB|[\cosh(s|Q_f eB|) - \cosh(su|Q_f eB|)]}{2\sinh^3(s|Q_f eB|)}\boldsymbol{k}^2_\perp \right. \\ & \left. + \frac{|Q_f eB|^2}{\sinh^2(s|Q_f eB|)}\right\},\end{aligned} \tag{20}$$

$$\begin{aligned}\Pi_{\sigma,\mathrm{vac}}(\boldsymbol{k}^2_\perp, \boldsymbol{k}^2_\parallel) = {} & \frac{N_c}{4\pi^2} \sum_{f=u,d} \int_0^\infty ds \int_0^1 du \exp\left[-m^2 s - \frac{s(1-u^2)}{4}\boldsymbol{k}^2_\parallel - \frac{\cosh(s|Q_f eB|) - \cosh(su|Q_f eB|)}{2|Q_f eB| \sinh(s|Q_f eB|)}\boldsymbol{k}^2_\perp\right] \\ & \times \left\{\left(-m^2 + \frac{1}{s} - \frac{1-u^2}{4}\boldsymbol{k}^2_\parallel\right)\frac{|Q_f eB|}{\tanh(s|Q_f eB|)} - \frac{|Q_f eB|[\cosh(s|Q_f eB|) - \cosh(su|Q_f eB|)]}{2\sinh^3(s|Q_f eB|)}\boldsymbol{k}^2_\perp \right. \\ & \left. + \frac{|Q_f eB|^2}{\sinh^2(s|Q_f eB|)}\right\}.\end{aligned} \tag{21}$$

Here, $\boldsymbol{k}_{\parallel}^2 = k_3^2 + k_4^2$ and $\boldsymbol{k}_{\perp}^2 = k_1^2 + k_2^2$. Note that we have made the Wick rotation $s \to -is$ and $k^0 \to ik_4$.

At finite temperature, after making Matsubara frequency summation [118,123] we obtain the polarization functions as follows:

$$\begin{aligned}\Pi_{\pi^0}(\omega_m^B, \boldsymbol{k}_{\perp}^2, k_3^2) =& \frac{N_c T}{4\sqrt{\pi^3}} \sum_{f=u,d} \sum_{l=-\infty}^{\infty} \int_0^{\infty} ds \int_{-1}^{1} du \sqrt{s} \exp\Big\{-s[(\omega_l^F)^2 + m^2] + s(1-u)\omega_l^F \omega_m^B - \frac{s}{2}(1-u)(\omega_m^B)^2 \\ &- \frac{s(1-u^2)}{4} k_3^2 - \frac{\cosh(s|Q_f eB|) - \cosh(su|Q_f eB|)}{2\sinh(s|Q_f eB|)} \frac{\boldsymbol{k}_{\perp}^2}{|Q_f eB|}\Big\}\Big\{\Big[m^2 + \frac{1}{2s} - i\omega_l^F(i\omega_l^F - i\omega_m^B) \\ &- \frac{1-u^2}{4} k_3^2\Big] \frac{|Q_f eB|}{\tanh(s|Q_f eB|)} + \frac{|Q_f eB|^2}{\sinh^2(s|Q_f eB|)} - \frac{|Q_f eB|[\cosh(s|Q_f eB|) - \cosh(su|Q_f eB|)]}{2\sinh^3(s|Q_f eB|)} \boldsymbol{k}_{\perp}^2\Big\}, \end{aligned} \tag{22}$$

$$\begin{aligned}\Pi_{\sigma}(\omega_m^B, \boldsymbol{k}_{\perp}^2, k_3^2) =& \frac{N_c T}{4\sqrt{\pi^3}} \sum_{f=u,d} \sum_{l=-\infty}^{\infty} \int_0^{\infty} ds \int_{-1}^{1} du \sqrt{s} \exp\Big\{-s[(\omega_l^F)^2 + m^2] + s(1-u)\omega_l^F \omega_m^B - \frac{s}{2}(1-u)(\omega_m^B)^2 \\ &- \frac{s(1-u^2)}{4} k_3^2 - \frac{\cosh(s|Q_f eB|) - \cosh(su|Q_f eB|)}{2\sinh(s|Q_f eB|)} \frac{\boldsymbol{k}_{\perp}^2}{|Q_f eB|}\Big\}\Big\{\Big[-m^2 + \frac{1}{2s} - i\omega_l^F(i\omega_l^F - i\omega_m^B) \\ &- \frac{1-u^2}{4} k_3^2\Big] \frac{|Q_f eB|}{\tanh(s|Q_f eB|)} + \frac{|Q_f eB|^2}{\sinh^2(s|Q_f eB|)} - \frac{|Q_f eB|[\cosh(s|Q_f eB|) - \cosh(su|Q_f eB|)]}{2\sinh^3(s|Q_f eB|)} \boldsymbol{k}_{\perp}^2\Big\}. \end{aligned} \tag{23}$$

Since we evaluate the screening masses, the Matsubara frequencies of bosons (mesons) $\omega_m^B = 2m\pi T$ with $m = 0, \pm 1, \pm 2 \ldots$, which emerge in Eqs. (22) and (23), should be vanished, namely, $k_4 = 0$. As shown in Ref. [104], the screening masses of mesons in a heat reservoir but with vanishing magnetic field can be calculated by making use of the dispersion relation obtained from Eq. (18), i.e.,

$$[1 - 2G\Pi_{\xi}(k_4 = 0, \boldsymbol{k}^2)]|_{\boldsymbol{k}^2 = -m_{\xi,\mathrm{scr}}^2} = 0, \quad \text{for } B \to 0, \tag{24}$$

where $\boldsymbol{k} = (k^1, k^2, k^3)$. And it was pointed out that, by using the prescription of Ref. [104], the meson screening masses $m_{\xi,\mathrm{scr}}$ are always less than the threshold mass $2\sqrt{m^2 + (\pi T)^2}$ at sufficiently high temperatures, so that they do not develop an imaginary part. In the presence of an external magnetic field, analogously, the longitudinal screening masses $m_{\xi,\mathrm{scr},\parallel}$ and the transverse screening masses $m_{\xi,\mathrm{scr},\perp}$ of the mesons are determined by

$$[1 - 2G\Pi_{\xi,\mathrm{vac}}(0, k_3^2)]|_{k_3^2 = -m_{\xi,\mathrm{scr},\parallel}^2} = 0 \tag{25}$$

and

$$[1 - 2G\Pi_{\xi,\mathrm{vac}}(\boldsymbol{k}_{\perp}^2, 0)]|_{\boldsymbol{k}_{\perp}^2 = -m_{\xi,\mathrm{scr},\perp}^2} = 0 \tag{26}$$

for $T = 0$ and by

$$[1 - 2G\Pi_{\xi}(0, 0, k_3^2)]|_{k_3^2 = -m_{\xi,\mathrm{scr},\parallel}^2} = 0 \tag{27}$$

and

$$[1 - 2G\Pi_{\xi}(0, \boldsymbol{k}_{\perp}^2, 0)]|_{\boldsymbol{k}_{\perp}^2 = -m_{\xi,\mathrm{scr},\perp}^2} = 0 \tag{28}$$

for $T \neq 0$.

Then, with the help of the method for regularizing the polarization functions in Ref. [63], we make an extension from the Pauli-Villars regularization scheme to the proper-time regularization scheme with the infrared cutoff Λ_{IR}. The explicit regularized expressions of the polarization functions at zero and finite temperature are changed to the forms as follows, respectively:

$$\begin{aligned}\Pi_{\xi,\mathrm{vac}}^{\mathrm{PT}}(\boldsymbol{k}_{\perp}^2, \boldsymbol{k}_3^2) =& 2\mathrm{I}_{1,\mathrm{vac}}^{\mathrm{PT}}(m^2) + (\boldsymbol{k}_{\parallel}^2 + 4m^2\epsilon_{\xi})\mathrm{I}_{2,\mathrm{vac},\parallel}^{\mathrm{PT}}(\boldsymbol{k}_{\perp}^2, \boldsymbol{k}_3^2) \\ &+ \boldsymbol{k}_{\perp}^2 \mathrm{I}_{2,\mathrm{vac},\perp}^{\mathrm{PT}}(\boldsymbol{k}_{\perp}^2, \boldsymbol{k}_3^2)\end{aligned} \tag{29}$$

and

$$\begin{aligned}\Pi_{\xi}^{\mathrm{PT}}(0, \boldsymbol{k}_{\perp}^2, k_3^2) =& 2\mathrm{I}_1^{\mathrm{PT}}(m^2) + (k_3^2 + 4m^2\epsilon_{\xi})\mathrm{I}_{2,\parallel}^{\mathrm{PT}}(0, \boldsymbol{k}_{\perp}^2, k_3^2) \\ &+ \boldsymbol{k}_{\perp}^2 \mathrm{I}_{2,\perp}^{\mathrm{PT}}(0, \boldsymbol{k}_{\perp}^2, k_3^2),\end{aligned} \tag{30}$$

where ϵ_{ξ} is defined by

$$\epsilon_{\xi} \equiv \begin{cases} 1, & \xi = \sigma, \\ 0, & \xi = \pi^0, \end{cases} \tag{31}$$

and

$$\mathrm{I}_{2,\mathrm{vac},\parallel}^{\mathrm{PT}}(\boldsymbol{k}_\perp^2,\boldsymbol{k}_3^2) = -\frac{N_c}{8\pi^2}\sum_{f=u,d}\int_{\frac{1}{\Lambda_{\mathrm{UV}}^2}}^{\frac{1}{\Lambda_{\mathrm{IR}}^2}} ds \int_0^1 du \exp\left[-m^2 s - \frac{s(1-u^2)}{4}\boldsymbol{k}_3^2 - \frac{\cosh(s|Q_f eB|) - \cosh(su|Q_f eB|)}{2|Q_f eB|\sinh(s|Q_f eB|)}\boldsymbol{k}_\perp^2\right] \times \frac{|Q_f eB|}{\tanh(s|Q_f eB|)}, \tag{32}$$

$$\mathrm{I}_{2,\mathrm{vac},\perp}^{\mathrm{PT}}(\boldsymbol{k}_\perp^2,\boldsymbol{k}_3^2) = -\frac{N_c}{8\pi^2}\sum_{f=u,d}\int_{\frac{1}{\Lambda_{\mathrm{UV}}^2}}^{\frac{1}{\Lambda_{\mathrm{IR}}^2}} du \exp\left[-m^2 s - \frac{s(1-u^2)}{4}\boldsymbol{k}_3^2 - \frac{\cosh(s|Q_f eB|) - \cosh(su|Q_f eB|)}{2|Q_f eB|\sinh(s|Q_f eB|)}\boldsymbol{k}_\perp^2\right] \times \frac{|Q_f eB|\cosh(su|Q_f eB|)}{\sinh(s|Q_f eB|)}, \tag{33}$$

$$\mathrm{I}_{2,\parallel}^{\mathrm{PT}}(0,\boldsymbol{k}_\perp^2,k_3^2) = -\frac{N_c}{4\sqrt{\pi^3}}\sum_{f=u,d}\int_{\frac{1}{\Lambda_{\mathrm{UV}}^2}}^{\frac{1}{\Lambda_{\mathrm{IR}}^2}} \int_0^1 du\sqrt{s} \exp\left[-m^2 s - \frac{s(1-u^2)}{4}k_3^2 - \frac{\cosh(s|Q_f eB|) - \cosh(su|Q_f eB|)}{2|Q_f eB|\sinh(s|Q_f eB|)}\boldsymbol{k}_\perp^2\right] \times [T\theta_2(0, e^{-4\pi^2 T^2 s})]\frac{|Q_f eB|}{\tanh(s|Q_f eB|)}, \tag{34}$$

and

$$\mathrm{I}_{2,\perp}^{\mathrm{PT}}(0,\boldsymbol{k}_\perp^2,k_3^2) = -\frac{N_c}{4\sqrt{\pi^3}}\sum_{f=u,d}\int_{\frac{1}{\Lambda_{\mathrm{UV}}^2}}^{\frac{1}{\Lambda_{\mathrm{IR}}^2}} \int_0^1 du\sqrt{s} \exp\left[-m^2 s - \frac{s(1-u^2)}{4}k_3^2 - \frac{\cosh(s|Q_f eB|) - \cosh(su|Q_f eB|)}{2|Q_f eB|\sinh(s|Q_f eB|)}\boldsymbol{k}_\perp^2\right] \times [T\theta_2(0, e^{-4\pi^2 T^2 s})]\frac{|Q_f eB|\cosh(su|Q_f eB|)}{\sinh(s|Q_f eB|)}. \tag{35}$$

It is easy to find out the anisotropy between the longitudinal and transverse directions in terms of Eqs. (29) and (30), since $\mathrm{I}_{2,\mathrm{vac},\parallel} \neq \mathrm{I}_{2,\mathrm{vac},\perp}$ and $\mathrm{I}_{2,\parallel} \neq \mathrm{I}_{2,\perp}$ at nonzero magnetic fields. Thus, the longitudinal screening masses are different from the transverse screening ones, i.e., $m_{\xi,\mathrm{scr},\parallel} \neq m_{\xi,\mathrm{scr},\perp}$, when the magnetic field is present. But when $eB \to 0$, we have $\lim_{eB\to 0}\mathrm{I}_{2,\mathrm{vac},\parallel} = \lim_{eB\to 0}\mathrm{I}_{2,\mathrm{vac},\perp}$ at $T=0$ and $\lim_{eB\to 0}\mathrm{I}_{2,\parallel} = \lim_{eB\to 0}\mathrm{I}_{2,\perp}$ at $T\neq 0$. It means that the Lorentz symmetry broken by the magnetic field is going to be restored, i.e., $SO(2)\otimes SO(1,1) \to SO(1,3)$ at zero temperature and $SO(2)\to SO(3)$ at finite temperature. Correspondingly, the relative index of refraction of the medium [75] becomes unity (i.e., $\frac{n_{\xi,\parallel}}{n_{\xi,\perp}} = \frac{m_{\xi,\mathrm{scr},\parallel}}{m_{\xi,\mathrm{scr},\perp}} = 1$) in the absence of the magnetic field, whether the system is in a heat reservoir or not.

IV. NUMERICAL RESULTS

A. The B-dependent coupling constant G

As mentioned above, it is an effective and convenient way to employ a magnetic-field-dependent four-fermion coupling constant in the NJL-type models, in order to incorporate inverse magnetic catalysis at high temperatures. Hence, by following Ref. [55], we determine the magnetic field dependence of the coupling constant G by using the magnetic-field-dependent constituent quark masses inferred from the baryon masses in the magnetic fields obtained by lattice simulations.

Specifically, we first fix the model parameters including the current quark mass m_0 and the ultraviolet cutoff Λ_{UV}, by setting the predictions of the model for the pion mass m_π and for its decay constant f_π to their physical values, i.e., 138 and 93 MeV, respectively. Then, to fix the magnetic-dependent coupling constant $G(eB)$, we set the constituent quark mass at each B to take the value inferred from the first-principles input of the baryon masses. Note that, in this paper, we introduce an infrared cutoff that provides the quark confinement to eliminate unphysical quark-antiquark thresholds for mesons. And the infrared cutoff $\Lambda_{\mathrm{IR}} = 240$ MeV which is approximately equal to Λ_{QCD}. The results of the fixed model parameters are $m_0 = 11.8$ MeV, $\Lambda_{\mathrm{UV}} = 708$ MeV, and $G(T=B=0)\Lambda_{\mathrm{UV}}^2 = 5.5$, and the values of the magnetic-field-dependent four-fermion coupling constant $G(eB)$, as well as the constituent quark masses used to fix them, are given in Table I. Moreover, the curve of the coupling constant G as a function of eB is also shown in Fig. 1, in comparison with that in Ref. [55]. Clearly, the coupling constant in our model decreases with increasing magnetic field, which is qualitatively in agreement with the results in Ref. [55]. And we need to emphasize that, although the authors in Ref. [55] worked in the Polyakov loop-extended NJL model (PNJL), they solely employed the input at zero temperature when fixing

TABLE I. The values of the magnetic-field-dependent coupling constant and the constituent quark masses used to fix them.

eB [GeV^2]	0.0	0.1	0.2	0.3	0.4	0.5	0.6	0.7
m^2 [GeV^2]	0.097	0.096	0.094	0.091	0.087	0.083	0.079	0.074
G [GeV^{-2}]	10.97	10.72	10.02	9.14	8.18	7.26	6.44	5.69

the magnetic field dependence of G, and thus the Polyakov loop contributed nothing.

B. The solution of the gap equation and the pseudocritical temperature T_{pc}

In this subsection, we show the results of the constituent quark mass and the quark condensate as functions of the temperature at different values of eB in the framework of both the standard NJL model and the lattice-improved NJL model, as shown in Figs. 2 and 3, respectively. It is found in Fig. 2 that, at a certain fixed temperature value, the constituent quark mass m decreases with eB in the lattice-improved NJL model with the magnetic-dependent coupling constant, while the situation is on the contrary in the standard NJL model with a constant $G(B=0)$.

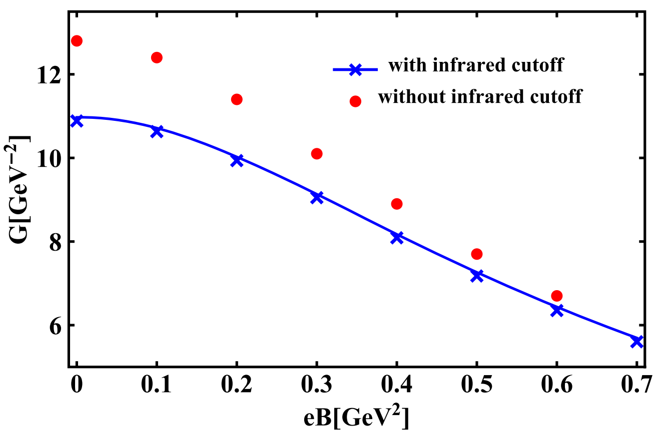

FIG. 1. The coupling constant G as a function of eB compared with the results in Ref. [55]. The blue line denotes the results in this paper, and the red dots denote the results in Ref. [55].

On the other hand, as depicted by Fig. 3, in the standard NJL model, the quark condensate increases with the magnetic field at any temperatures, which is just referred to as magnetic catalysis. However, in the case of the lattice-improved NJL model, the quark condensate curves display magnetic catalysis only at low temperatures but show inverse magnetic catalysis at sufficiently high temperatures around the transition, which is consistent with the lattice results in Ref. [19]. Note that the same values of eB as Ref. [55] are chosen for convenience in our calculations when we evaluate the constituent quark mass and the quark condensate.

Using the results of the quark condensates in Fig. 3, we plot the pseudocritical temperature T_{pc}, defined by the location of the inflection points of the quark condensate curves, as a function of the magnetic field strength in Fig. 4. It is obvious that our numerical results of $T_{\mathrm{pc}}(B)$ in the lattice-improved NJL model are qualitatively in good agreement with the lattice results in Ref. [18] as opposed to the standard NJL model. As shown in Ref. [55], the authors actually used the PNJL model with magnetic-field-dependent G to reproduce the IMC successfully. Our numerical results in the lattice-improved NJL model without the Polyakov loop are still consistent with those in Ref. [55]. It implies that the key point for introducing IMC in the NJL-type models is the magnetic-field-dependent four-fermion coupling constant and the Polyakov loop is

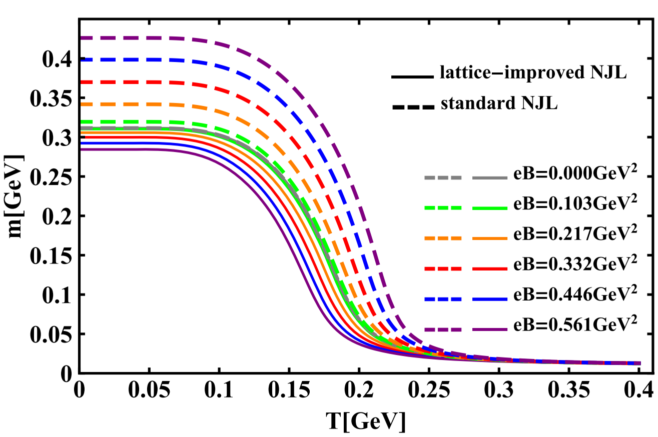

FIG. 2. The constituent quark mass as a function of the temperature at different eB compared with the results of standard NJL model.

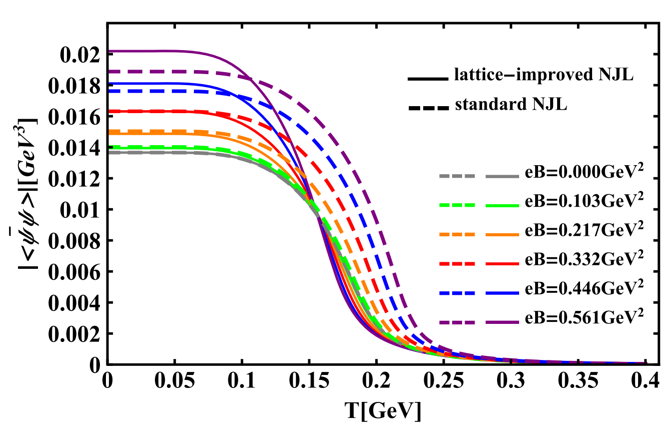

FIG. 3. The absolute value of the quark condensate as a function of the temperature at different eB compared with the standard NJL model.

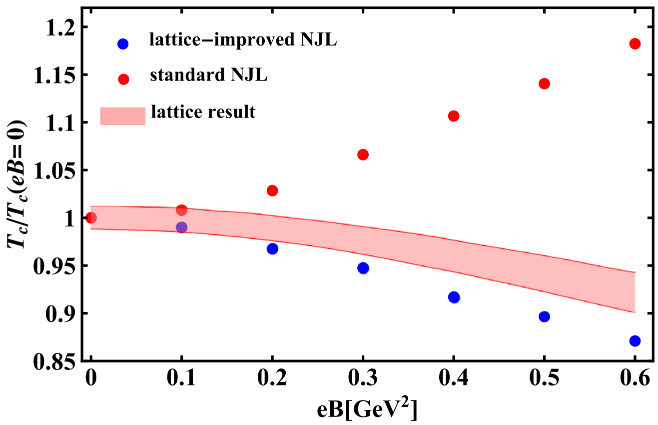

FIG. 4. The pseudocritical temperature scaled by its $eB = 0$ value as a function of the magnetic field compared with the results from lattice simulations [18].

not essential. For this reason, our robust lattice-improved NJL model is qualified to investigate the effects of the IMC on the screening masses of mesons.

C. The screening masses of neutral pion and sigma meson

1. Results at fixed eB

The screening masses of neutral pions and sigma mesons can be evaluated in terms of Eqs. (25)–(28). Now we begin the discussion with the results of their screening masses as functions of the temperature at different values of eB in the cases of the standard NJL model and the lattice-improved NJL model.

For the standard NJL model, the temperature dependences of the longitudinal and transverse screening masses for π^0 and σ mesons at fixed $eB = 0.0$, 0.2, 0.4, and 0.6 GeV^2 are shown in the left panels in Figs. 5 and 6, respectively. In general, the curves of longitudinal screening masses show similar behavior with those of transverse ones. At low temperatures ($T \lesssim 150$ MeV), the longitudinal and transverse screening masses of both π^0 and σ mesons hardly change with the increase of temperature. As the temperature becomes higher and higher, the longitudinal and transverse screening masses of neutral pions

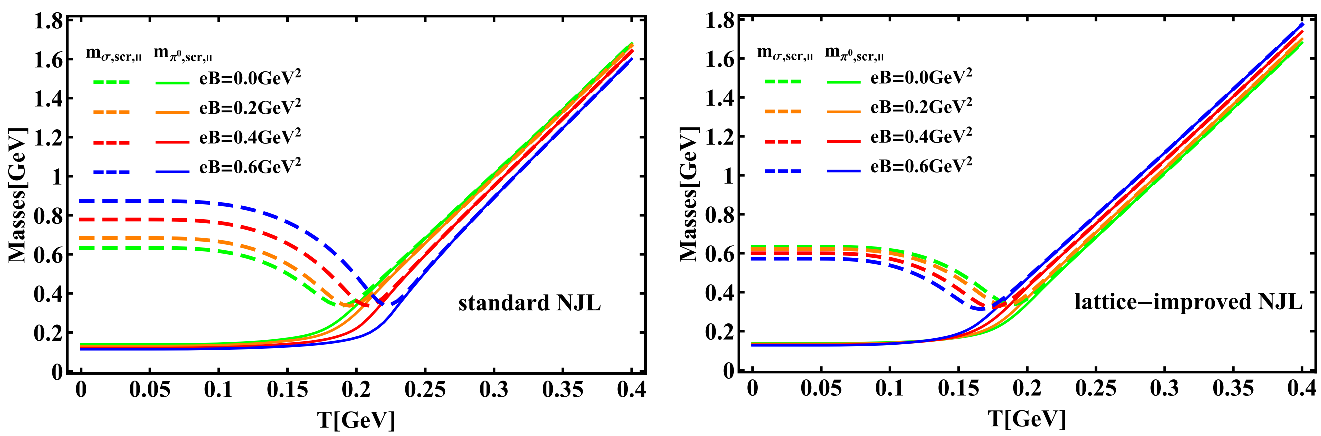

FIG. 5. Left panel: the longitudinal meson screening masses as functions of the temperature at fixed $eB = 0.0$, 0.2, 0.4, and 0.6 GeV^2 in the standard NJL model. Right panel: the same quantities in the lattice-improved NJL model.

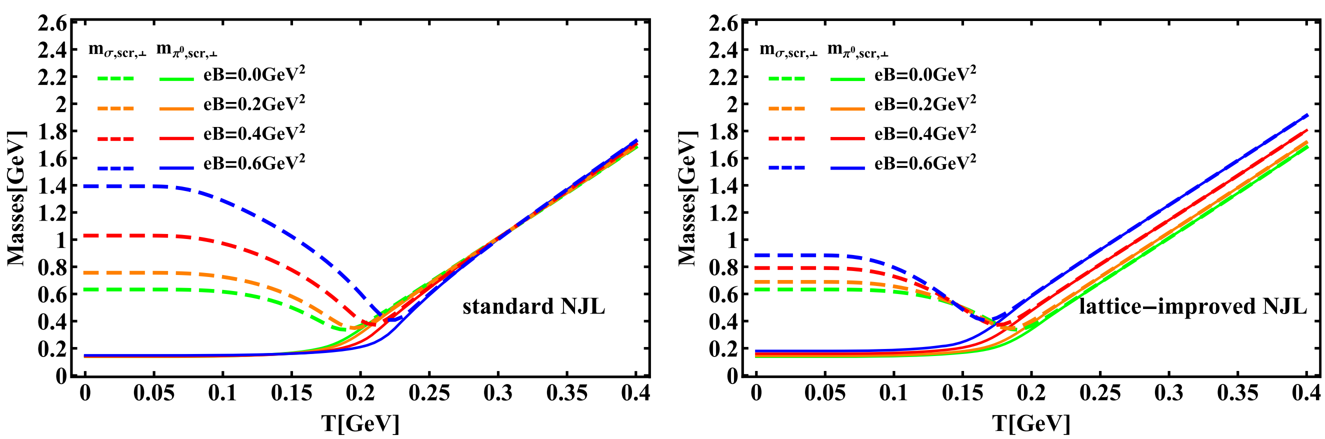

FIG. 6. Left panel: the transverse meson screening masses as functions of the temperature at fixed $eB = 0.0$, 0.2, 0.4, and 0.6 GeV^2 in the standard NJL model. Right panel: the same quantities in the lattice-improved NJL model.

begin to increase with the increasing temperature T, while both screening masses of sigma mesons first decrease and then increase as T is growing. Especially, at a certain temperature, defined by $T_\chi^\parallel$ (or $T_\chi^\perp$), the longitudinal (or transverse) screening masses of neutral pions and sigma mesons merge with each other. This phenomenon implies that the chiral symmetry is restored at $T_\chi^\parallel$ (or $T_\chi^\perp$), because neutral pion and sigma mesons are chiral partners. And it is shown that the merging temperature, either $T_\chi^\parallel$ or $T_\chi^\perp$, is enhanced by the magnetic field.

As for our lattice-improved NJL model, the corresponding numerical results of the meson screening masses are shown in the right panels in Figs. 5 and 6. By comparing with the results in the standard NJL model, we could examine the effects of the IMC on the meson screening masses. First, as shown by Fig. 5, it is evident that $m_{\sigma,\mathrm{scr},\parallel}$ obtained in the lattice-improved NJL model is reduced by the magnetic field at low temperatures but is changed to increase with B at high temperatures, in contrast to the standard NJL. Second, as regard to $m_{\sigma,\mathrm{scr},\perp}$, as shown in Fig. 6, it remains enhanced by the magnetic field at low temperatures in the lattice-improved NJL model, although the extent of the increment is less than that in the standard NJL model. However, while T is around $T_\chi^\perp$, $m_{\sigma,\mathrm{scr},\perp}$ acquired by the lattice-improved NJL model increases with B, similar to $m_{\sigma,\mathrm{scr},\parallel}$. Third, more importantly, when approaching $T_\chi^\parallel$ ($T_\chi^\perp$), the results of the lattice-improved NJL model show that the larger the strength of the magnetic field, the lower the temperature where either $m_{\sigma,\mathrm{scr},\parallel}$ ($m_{\sigma,\mathrm{scr},\perp}$) or $m_{\pi^0,\mathrm{scr},\parallel}$ ($m_{\pi^0,\mathrm{scr},\perp}$) starts to increase with T remarkably, as opposed to the results in the standard NJL. Consequently, the location where the two curves of the screening masses of neutral pions and sigma mesons merge together moves toward the vertical axis with the enhancement of the magnetic field. That is to say, $T_\chi^\parallel$ ($T_\chi^\perp$) is reduced by the increase of the magnetic field strength in the case of our lattice-improved NJL model. In addition, it is obvious that, in the high-temperature limit, the curves of $m_{\sigma,\mathrm{scr},\perp}$ (or $m_{\pi^0,\mathrm{scr},\perp}$) at different values of eB in the standard NJL tend to approach each other as T grows, while those curves in the lattice-improved NJL model keep increasing with T separately and parallelly.

Since the neutral pions and the sigma mesons are chiral partners with each other, we could introduce their screening mass difference to investigate the chiral phase transition as an alternative of the chiral condensate, as we have discussed above. Explicitly, the normalized screening mass difference between π^0 and σ mesons in the longitudinal and the transverse directions is defined by

$$\Delta\bar{M}^\parallel_{\sigma,\pi^0}(B,T) = \frac{\Delta m^\parallel_{\sigma,\pi^0}(B,T)}{\Delta m^\parallel_{\sigma,\pi^0}(0,0)} \tag{36}$$

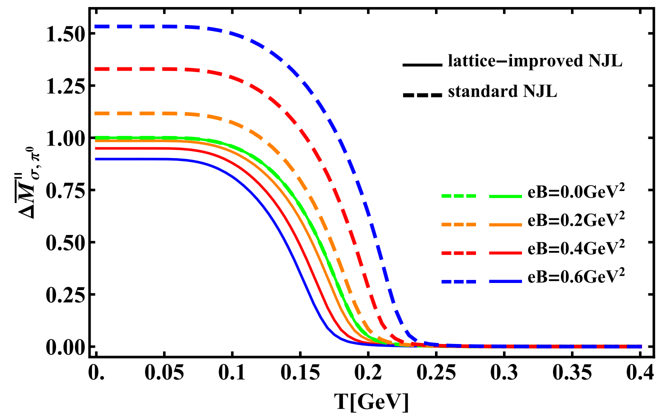

FIG. 7. The normalized longitudinal screening mass difference $\Delta\bar{M}^\parallel_{\sigma,\pi^0}$ as a function of the temperature at fixed $eB = 0.0$, 0.2, 0.4, and 0.6 GeV^2.

and

$$\Delta\bar{M}^\perp_{\sigma,\pi^0}(B,T) = \frac{\Delta m^\perp_{\sigma,\pi^0}(B,T)}{\Delta m^\perp_{\sigma,\pi^0}(0,0)}, \tag{37}$$

respectively, where $\Delta m^\parallel_{\sigma,\pi^0} = m_{\sigma,\mathrm{scr},\parallel} - m_{\pi^0,\mathrm{scr},\parallel}$ and $\Delta m^\perp_{\sigma,\pi^0} = m_{\sigma,\mathrm{scr},\perp} - m_{\pi^0,\mathrm{scr},\perp}$. And in Figs. 7 and 8, we display the normalized difference $\Delta\bar{M}^\parallel_{\sigma,\pi^0}$ and $\Delta\bar{M}^\perp_{\sigma,\pi^0}$ as functions of the temperature at $eB = 0.0$, 0.2, 0.4, and 0.6 GeV^2.

It is shown that, compared with Figs. 2 and 3, the temperature dependences of $\Delta\bar{M}^\parallel_{\sigma,\pi^0}$ and $\Delta\bar{M}^\perp_{\sigma,\pi^0}$ at different fixed values of eB are analogous to those of the constituent quark mass and the chiral condensate, respectively, no matter in the standard NJL model or the lattice-improved NJL model. Concretely, at low temperatures ($T \lesssim 100$ MeV), $\Delta\bar{M}^\parallel_{\sigma,\pi^0}$ or $\Delta\bar{M}^\perp_{\sigma,\pi^0}$ is nearly a constant with respect to the temperature in both the standard NJL

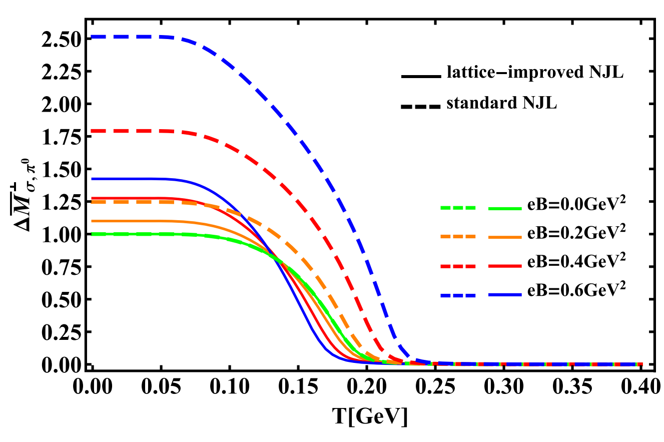

FIG. 8. The normalized transverse screening mass difference $\Delta\bar{M}^\perp_{\sigma,\pi^0}$ as a function of the temperature at fixed $eB = 0.0$, 0.2, 0.4, and 0.6 GeV^2.

model and the lattice-improved NJL model. In the interval of $100\ \mathrm{MeV} \lesssim T \lesssim 200\ \mathrm{MeV}$, the value of $\Delta\bar{M}^{\parallel}_{\sigma,\pi^0}$ or $\Delta\bar{M}^{\perp}_{\sigma,\pi^0}$ is sharply depressed by the growth of the temperature, which means that the chiral symmetry is restoring in this temperature range. At very high temperatures ($T \gtrsim 200$ MeV), the screening masses of π^0 and σ mesons become degenerate with a good approximation, i.e., $\Delta\bar{M}^{\parallel}_{\sigma,\pi^0} = 0$ or $\Delta\bar{M}^{\perp}_{\sigma,\pi^0} = 0$, and this fact signifies the restoration of chiral symmetry accordingly. Therefore, we can resort to the meson screening mass difference $\Delta\bar{M}^{\parallel}_{\sigma,\pi^0}$ (or $\Delta\bar{M}^{\perp}_{\sigma,\pi^0}$) as an order parameter instead of the quark condensate to define the critical temperature of the chiral phase transition.

Note that we define two critical temperatures by using the $\pi^0 - \sigma$ screening mass difference: One is the inflection point of $\Delta\bar{M}^{\parallel}_{\sigma,\pi^0}$ (or $\Delta\bar{M}^{\perp}_{\sigma,\pi^0}$) curve, which is identified with the pseudocritical temperature $T^{\parallel}_{\rm pc}$ (or $T^{\perp}_{\rm pc}$) of the chiral crossover, in analogy to the prescription for the quark condensate, namely,

$$\frac{\partial^2 \Delta\bar{M}^{\parallel}_{\sigma,\pi^0}}{\partial T^2}\bigg|_{T=T^{\parallel}_{\rm pc}} = 0 \quad \text{or} \quad \frac{\partial^2 \Delta\bar{M}^{\perp}_{\sigma,\pi^0}}{\partial T^2}\bigg|_{T=T^{\perp}_{\rm pc}} = 0, \qquad (38)$$

and the other is the merging point of $m_{\pi^0,\mathrm{scr},\parallel}$ (or $m_{\pi^0,\mathrm{scr},\perp}$) and $m_{\sigma,\mathrm{scr},\parallel}$ (or $m_{\sigma,\mathrm{scr},\perp}$), which is the critical temperature $T^{\parallel}_{\chi}$ (or $T^{\perp}_{\chi}$) signifying the chiral symmetry restoration, and the definition reads

$$\Delta\bar{M}^{\parallel}_{\sigma,\pi^0}|_{T=T^{\parallel}_{\chi}} = 0 \quad \text{or} \quad \Delta\bar{M}^{\perp}_{\sigma,\pi^0}|_{T=T^{\perp}_{\chi}} = 0. \qquad (39)$$

Nevertheless, since the chiral phase transition is actually a crossover owing to nonzero current quark mass, a small arbitrary value ϵ can be chosen to determine the critical temperatures $T^{\parallel}_{\chi}$ and $T^{\perp}_{\chi}$, e.g., $\Delta\bar{M}^{\parallel}_{\sigma,\pi^0}|_{T=T^{\parallel}_{\chi}} = \Delta\bar{M}^{\perp}_{\sigma,\pi^0}|_{T=T^{\perp}_{\chi}} = \epsilon = 10^{-2}$ in our numerical calculations. With the help of $T^{\parallel}_{\rm pc}$ ($T^{\perp}_{\rm pc}$) and $T^{\parallel}_{\chi}$ ($T^{\perp}_{\chi}$), the effects of the external magnetic field on these critical temperatures can be analyzed in the following.

On the one hand, the pseudocritical temperatures $T^{\parallel}_{\rm pc}$ and $T^{\perp}_{\rm pc}$ as functions of the magnetic field are shown in Fig. 9. And the pseudocritical temperature $T_{\rm pc}$ defined by the inflection points of the quark condensate from Fig. 3 is also sketched for comparison. In general, the eB dependences of $T^{\parallel}_{\rm pc}$ and $T^{\perp}_{\rm pc}$ are essentially coincident with that of $T_{\rm pc}$ not only in the standard NJL model but also in the lattice-improved NJL model, although somewhat less than $T_{\rm pc}$. It means that the normalized screening mass difference $\Delta\bar{M}^{\parallel}_{\sigma,\pi^0}$ and $\Delta\bar{M}^{\perp}_{\sigma,\pi^0}$ can effectively describe the chiral phase transition also. Evidently, in the left panel in Fig. 9, the value of $T^{\parallel}_{\rm pc}$ ($T^{\perp}_{\rm pc}$) becomes larger and larger with the increase of the magnetic field, which is in agreement with the result obtained by the quark condensate in the standard NJL model, whereas, in the right panel in Fig. 9, the decrease of $T^{\parallel}_{\rm pc}$ ($T^{\perp}_{\rm pc}$) with the increasing eB reflects the IMC from the LQCD simulations.

On the other hand, the eB dependences of $T^{\parallel}_{\chi}$ and $T^{\perp}_{\chi}$ are sketched in Fig. 10. The behaviors of them are quite similar to those of the pseudocritical temperatures in Fig. 9, although the values of $T^{\parallel}_{\chi}$ ($T^{\perp}_{\chi}$) are obviously larger than $T^{\parallel}_{\rm pc}$ ($T^{\perp}_{\rm pc}$) in both the standard NJL model and the lattice-improved NJL model. In the left panel in Fig. 10, the increase of $T^{\parallel}_{\chi}$ and $T^{\perp}_{\chi}$ with the growing eB reflects the MC in the standard NJL model. In the right panel in Fig. 10, their opposite behaviors varying with eB indicate the IMC effect, which can be well reproduced in the lattice-improved NJL model. Additionally, $T^{\parallel}_{\rm pc}$ is almost the same as $T^{\perp}_{\rm pc}$ at any value of eB as shown in Fig. 9, since they have nothing to do with the anisotropy of spacetime caused by the external magnetic field. By comparison, in Fig. 10, the difference between $T^{\parallel}_{\chi}$ and $T^{\perp}_{\chi}$ becomes larger and larger as

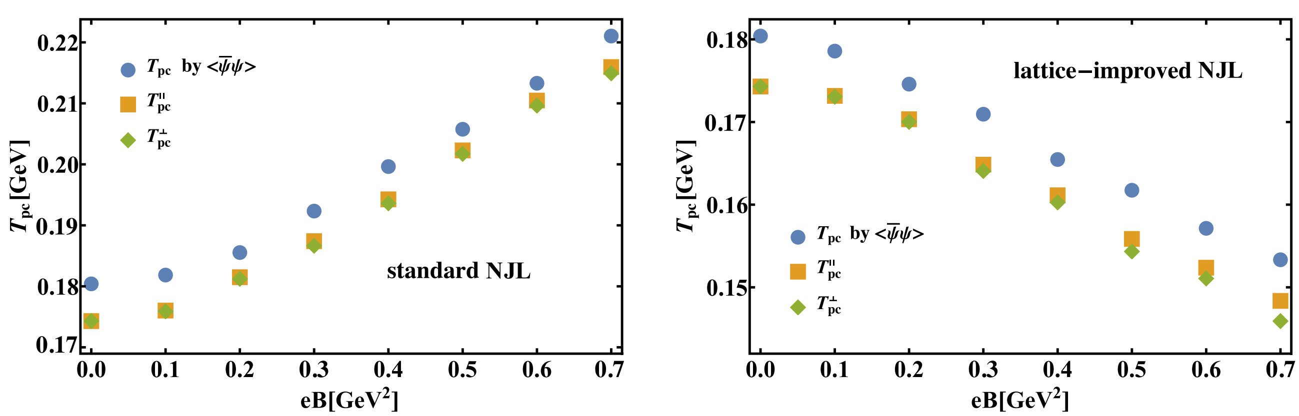

FIG. 9. The pseudocritical temperatures $T^{\parallel}_{\rm pc}$ and $T^{\perp}_{\rm pc}$, as well as $T_{\rm pc}$, as functions of eB in the standard (left panel) and the lattice-improved (right panel) NJL models.

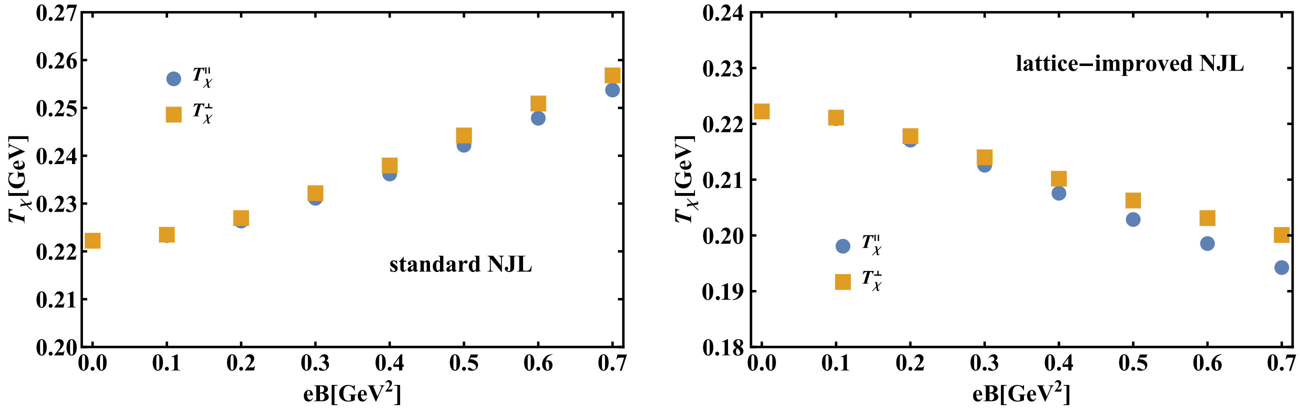

FIG. 10. The critical temperatures $T_\chi^{\parallel}$ and $T_\chi^{\perp}$, as functions of eB in the standard (left panel) and the lattice-improved (right panel) NJL models.

eB increases, and $T_\chi^{\perp}$ is always not less than $T_\chi^{\parallel}$. This is because of the definitions of $T_\chi^{\parallel}$ and $T_\chi^{\perp}$ in the latter case: It is not difficult to find that, in the low-momentum expansion,

$$m^2_{\sigma,\mathrm{scr},\parallel} - m^2_{\pi^0,\mathrm{scr},\parallel} = 4m^2 \tag{40}$$

and

$$m^2_{\sigma,\mathrm{scr},\perp} - m^2_{\pi^0,\mathrm{scr},\perp} = 4m^2 \times \frac{\mathrm{I}_{2,\parallel}(0)}{\mathrm{I}_{2,\perp}(0)}, \tag{41}$$

where $\mathrm{I}_{2,\parallel}(0) = \lim_{q\to 0}\mathrm{I}_{2,\parallel}(q)$ and $\mathrm{I}_{2,\perp}(0) = \lim_{q\to 0}\mathrm{I}_{2,\perp}(q)$, which are good approximations in the low-temperature region [75]. In this ansatz, we could have $\frac{(m^2_{\sigma,\mathrm{scr},\perp} - m^2_{\pi^0,\mathrm{scr},\perp})}{(m^2_{\sigma,\mathrm{scr},\parallel} - m^2_{\pi^0,\mathrm{scr},\parallel})} = \frac{\mathrm{I}_{2,\parallel}(0)}{\mathrm{I}_{2,\perp}(0)} \geq 1$ and, thus, $\frac{T_\chi^{\perp}}{T_\chi^{\parallel}} \geq 1$, both of which grow with the increase of eB.

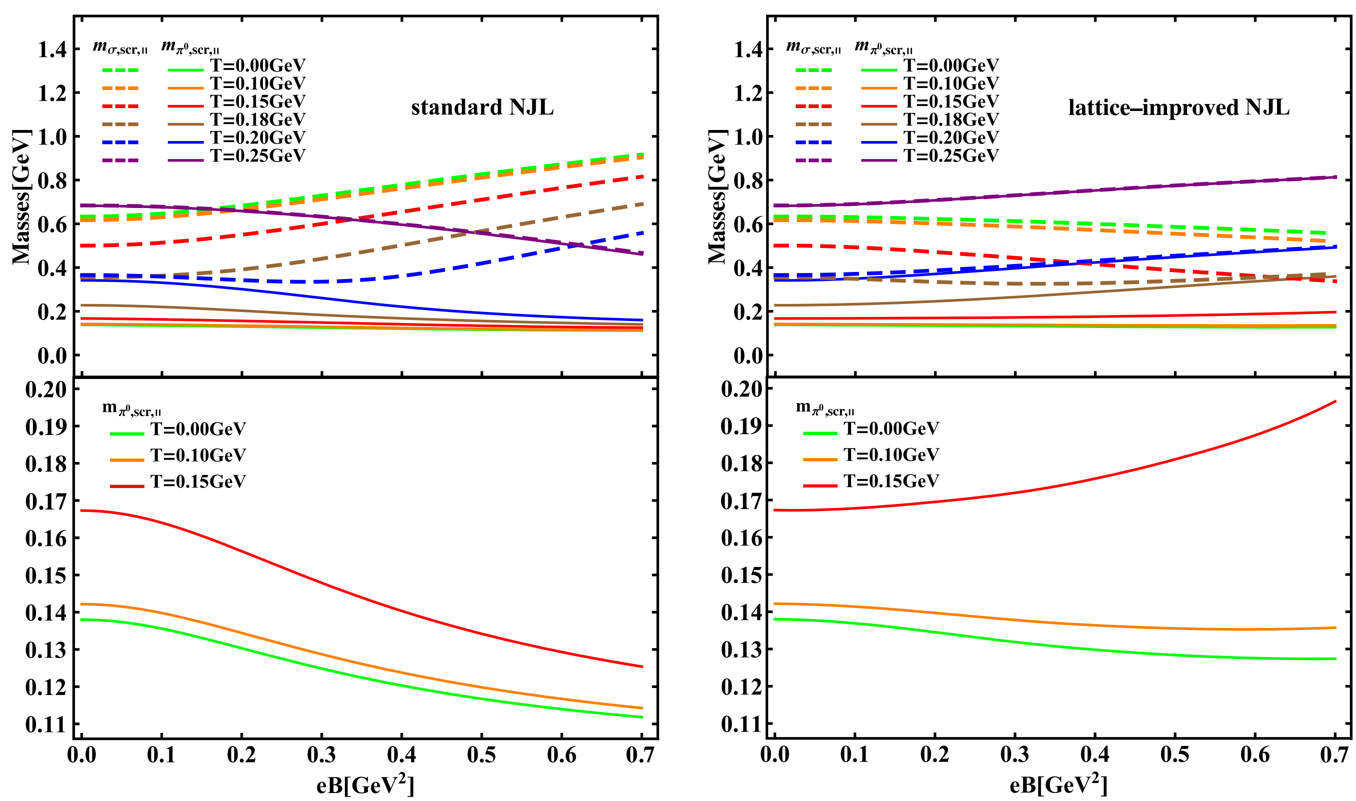

FIG. 11. Left panel: the longitudinal screening masses of π^0 and σ mesons as functions of eB at fixed $T = 0.00, 0.10, 0.15, 0.18, 0.20$, and 0.25 GeV in the standard NJL model, and the curves for neutral pion at low temperatures are plotted on the bottom for visibility. Right panel: the same quantities in the lattice-improved NJL model.

2. Results at fixed T

In this subsection, we first continue to present the eB dependences of $m_{\pi^0,\mathrm{scr},\parallel}$ and $m_{\sigma,\mathrm{scr},\parallel}$ at fixed $T = 0.00$, 0.10, 0.15, 0.18, 0.20, and 0.25 GeV in Fig. 11, in order to illustrate the effects of the IMC on the meson screening masses further. Specifically, in the standard NJL model, $m_{\pi^0,\mathrm{scr},\parallel}$ reduces monotonically with the growth of eB at either low or high temperatures, while in the lattice-improved NJL model, $m_{\pi^0,\mathrm{scr},\parallel}$ still decreases with eB at low temperatures (e.g., at $T = 0$ MeV and $T = 100$ MeV), despite that the extents of the decrease are smaller than those in the standard NJL model, but when the temperature is high enough (e.g., $T \geq 150$ MeV), $m_{\pi^0,\mathrm{scr},\parallel}$ turns to increase with eB.

As concerning $m_{\sigma,\mathrm{scr},\parallel}$, it is interesting to find that $m_{\sigma,\mathrm{scr},\parallel}$ increases in the standard NJL model but decreases in the lattice-improved NJL model at low temperatures, as eB grows. This is because, according to Eq. (40), since $m_{\pi^0,\mathrm{scr},\parallel}$ is almost a constant with respect to eB at $T \lesssim 150$ MeV, the behavior of $m_{\sigma,\mathrm{scr},\parallel}$ is mainly determined by that of the constituent quark mass m, and m in the lattice-improved NJL model decreases with eB as a result of the decreasing behavior of $G(eB)$ with regard to eB, in contrast to m in the standard NJL model. At very high temperatures, e.g., $T = 250$ MeV, $m_{\sigma,\mathrm{scr},\parallel}$ obviously becomes degenerate with $m_{\pi^0,\mathrm{scr},\parallel}$ and decreases in the standard NJL model but increases in the lattice-improved NJL model with the increase of eB instead. When around the chiral crossover, we find that $m_{\sigma,\mathrm{scr},\parallel}$ increases with eB at $T = 180$ MeV and first slightly decreases and then increases with eB at $T = 200$ MeV in the standard NJL model, as shown in the left panel in Fig. 11. However, as depicted by the right panel in Fig. 11, $m_{\sigma,\mathrm{scr},\parallel}$ first slightly decreases and then increases with eB at $T = 180$ MeV and turns to increase with eB monotonically at $T = 200$ MeV in the lattice-improved NJL model.

Next, the plots of $m_{\pi^0,\mathrm{scr},\perp}$ and $m_{\sigma,\mathrm{scr},\perp}$ as functions of eB at fixed temperatures are shown in Fig. 12. One interesting thing is that at low temperatures (i.e., $T = 0$ and 100 MeV), $m_{\pi^0,\mathrm{scr},\perp}$ either in the standard NJL model or in the lattice-improved NJL model is enhanced by the magnetic field, in contrast to $m_{\pi^0,\mathrm{scr},\parallel}$. But the rising of temperature makes the situation different: In the standard NJL model, $m_{\pi^0,\mathrm{scr},\perp}$ turns to first decrease and then increase with the increasing of eB at $T = 150$ MeV and eventually becomes reduced with eB at high temperatures (e.g., $T = 180$, 200, and 250 MeV); while in the lattice-improved NJL model, $m_{\pi^0,\mathrm{scr},\perp}$ remains increasing with eB as the temperature grows. As for $m_{\sigma,\mathrm{scr},\perp}$, when in the standard NJL model, the eB dependences of $m_{\sigma,\mathrm{scr},\perp}$ at different temperatures are

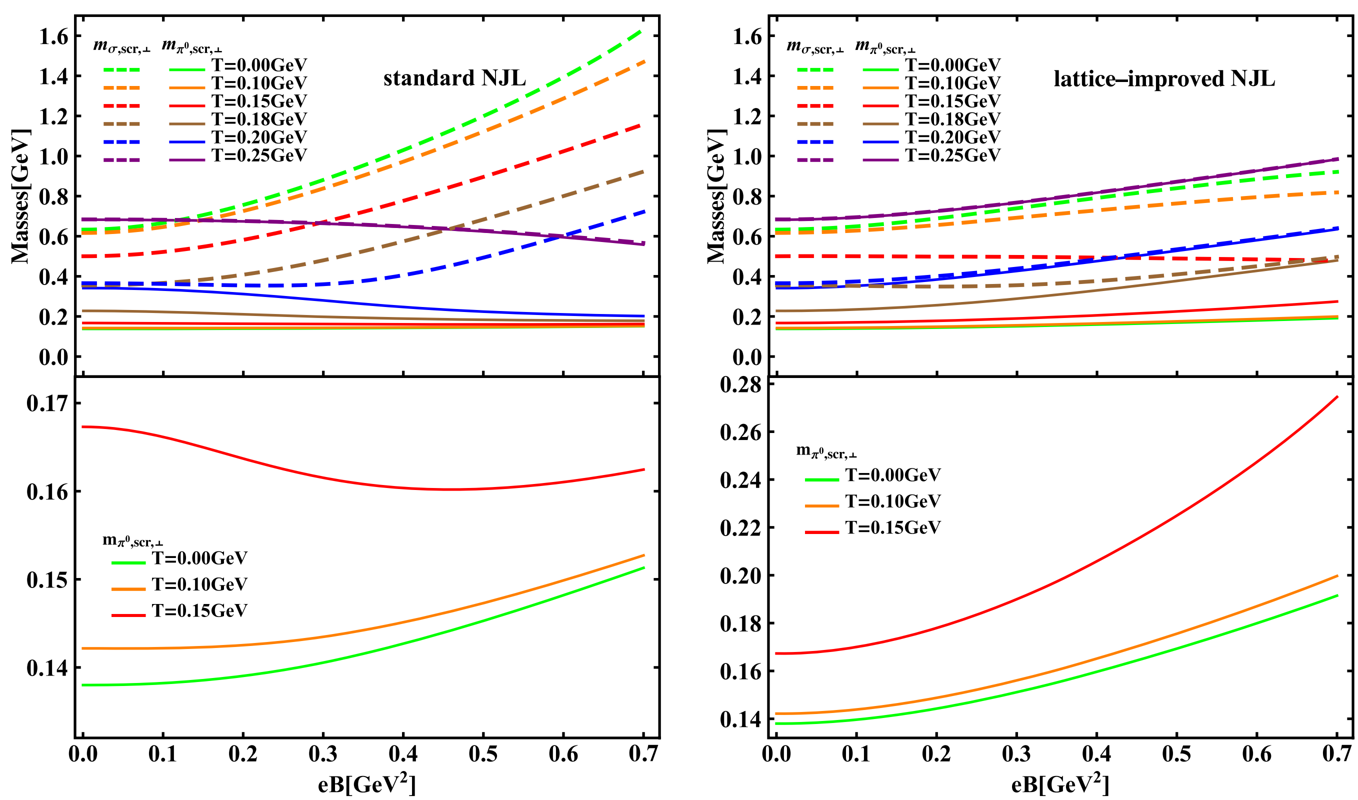

FIG. 12. Left panel: the transverse screening masses of π^0 and σ mesons as functions of eB at fixed $T = 0.00$, 0.10, 0.15, 0.18, 0.20, and 0.25 GeV in the standard NJL model, and the curves for neutral pion at low temperatures are plotted on the bottom for visibility. Right panel: the same quantities in the lattice-improved NJL model.

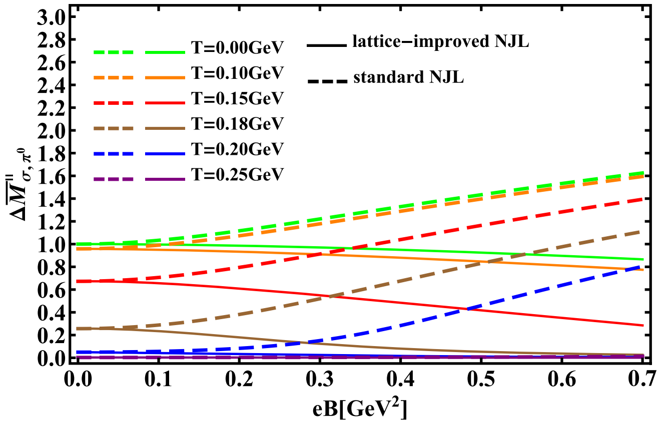

FIG. 13. The normalized longitudinal screening mass difference $\Delta\bar{M}^{\parallel}_{\sigma,\pi^0}$ as a function of eB at fixed $T = 0.0$, 0.10, 0.15, 0.18, 0.20, and 0.25 GeV.

qualitatively similar to those of $m_{\sigma,\mathrm{scr},\parallel}$. On the other hand, when in the lattice-improved NJL model, although $m_{\sigma,\mathrm{scr},\perp}$ and $m_{\sigma,\mathrm{scr},\parallel}$ behave similarly to each other as eB increases at enough high temperatures ($T \gtrsim 150$ MeV), there are some difference between them at low temperatures (e.g., $T = 0$ and 100 MeV): $m_{\sigma,\mathrm{scr},\perp}$ increases with eB, while $m_{\sigma,\mathrm{scr},\parallel}$ holds decreasing with eB.

Then, by making use of the numerical results in Figs. 11 and 12, we examine the eB dependences of $\Delta\bar{M}^{\parallel}_{\sigma,\pi^0}$ and $\Delta\bar{M}^{\perp}_{\sigma,\pi^0}$ at different temperatures in Figs. 13 and 14, respectively. Obviously, in the standard NJL model, only magnetic catalysis can be uncovered by $\Delta\bar{M}^{\parallel}_{\sigma,\pi^0}$ and $\Delta\bar{M}^{\perp}_{\sigma,\pi^0}$ that are enhanced by the increase of eB at arbitrary temperature. However, both of them decrease with the increasing eB at high temperatures (below $T^{\parallel}_{\chi}$ or $T^{\perp}_{\chi}$, of course) in the lattice-improved NJL model, which is consistent with the corresponding inverse magnetic catalysis acquired by the chiral condensate. Moreover, at low temperatures, it is not difficult to find that, in both the standard and the lattice-improved NJL models, $\Delta\bar{M}^{\parallel}_{\sigma,\pi^0}$ shows the same eB dependence as m according to Eq. (40), while $\Delta\bar{M}^{\perp}_{\sigma,\pi^0}$ acts much like the quark condensate as eB grows.

Furthermore, by comparing Fig. 11 with Fig. 12, we can find there are quantitative differences between $m_{\pi^0,\mathrm{scr},\parallel}$ ($m_{\sigma,\mathrm{scr},\parallel}$) and $m_{\pi^0,\mathrm{scr},\perp}$ ($m_{\sigma,\mathrm{scr},\perp}$) at fixed temperature in the same model, which are related to the anisotropy of spacetime caused by the background magnetic field and will be discussed in the following subsection.

D. The ratio of sound velocities $u^{\perp}_{\xi}/u^{\parallel}_{\xi}$

As mentioned in Ref. [75], the degree of the asymmetry between the longitudinal and transverse directions, stemming from the external magnetic field, can be measured by the ratio of sound velocities $u^{\perp}_{\xi}/u^{\parallel}_{\xi} = m_{\xi,\mathrm{scr},\parallel}/m_{\xi,\mathrm{scr},\perp}$, with the definitions $u^{\parallel}_{\xi} = \frac{m_{\xi,\mathrm{pole}}}{m_{\xi,\mathrm{scr},\parallel}}$ and $u^{\perp}_{\xi} = \frac{m_{\xi,\mathrm{pole}}}{m_{\xi,\mathrm{scr},\perp}}$. Thus, Figs. 15 and 16 show the T and eB dependences of the ratio $u^{\perp}_{\xi}/u^{\parallel}_{\xi}$ for $\xi = \pi^0$ and σ mesons, respectively. According to our arguments about the Lorentz symmetry breaking and the causality in Ref. [75], it is expected that $u^{\perp}_{\xi}/u^{\parallel}_{\xi} = 1$ at $eB = 0$ and $u^{\perp}_{\xi}/u^{\parallel}_{\xi} < 1$ at $eB \neq 0$ at zero and finite temperature, which are in agreement with the results in Figs. 15 and 16. Furthermore, $u^{\perp}_{\pi^0}/u^{\parallel}_{\pi^0}$ and $u^{\perp}_{\sigma}/u^{\parallel}_{\sigma}$ are both reduced by the increasing eB because of the enhancement of the symmetry breaking in coordinate space by the magnetic field, no matter in the standard NJL model or in the lattice-improved NJL model. Note that the eB dependence of $u^{\perp}_{\pi^0}/u^{\parallel}_{\pi^0}$ in the standard NJL model, as shown in the left panel in Fig. 16, is qualitatively in accordance with the result in Ref. [75].

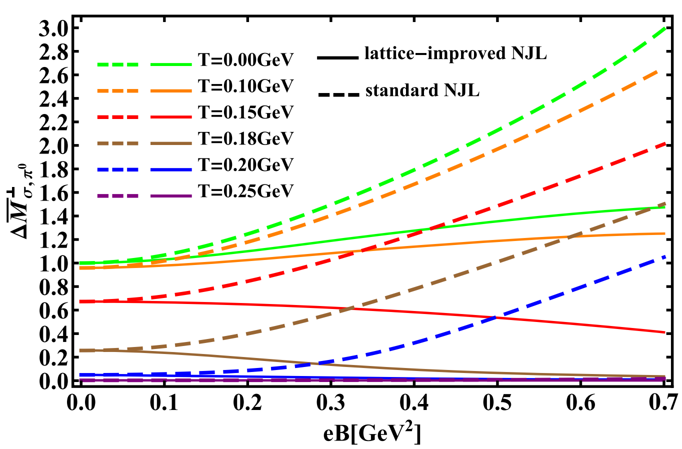

FIG. 14. The normalized transverse screening mass difference $\Delta\bar{M}^{\perp}_{\sigma,\pi^0}$ as a function of eB at fixed $T = 0.0$, 0.10, 0.15, 0.18, 0.20, and 0.25 GeV.

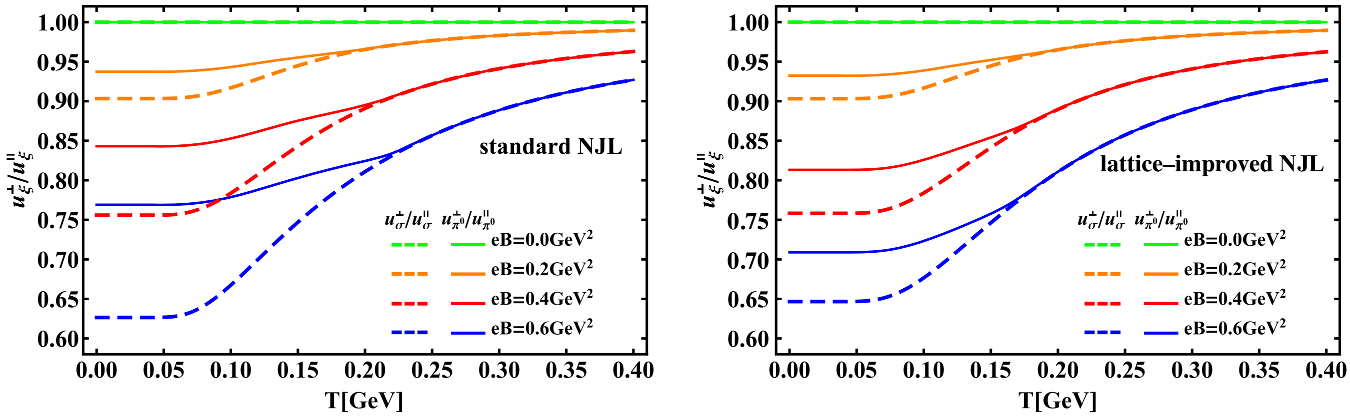

FIG. 15. $u_\xi^\perp/u_\xi^\parallel$ as a function of T at fixed $eB = 0.0$, 0.2, 0.4, and 0.6 GeV^2 in the standard NJL model (left panel) and the lattice-improved NJL model (right panel), respectively.

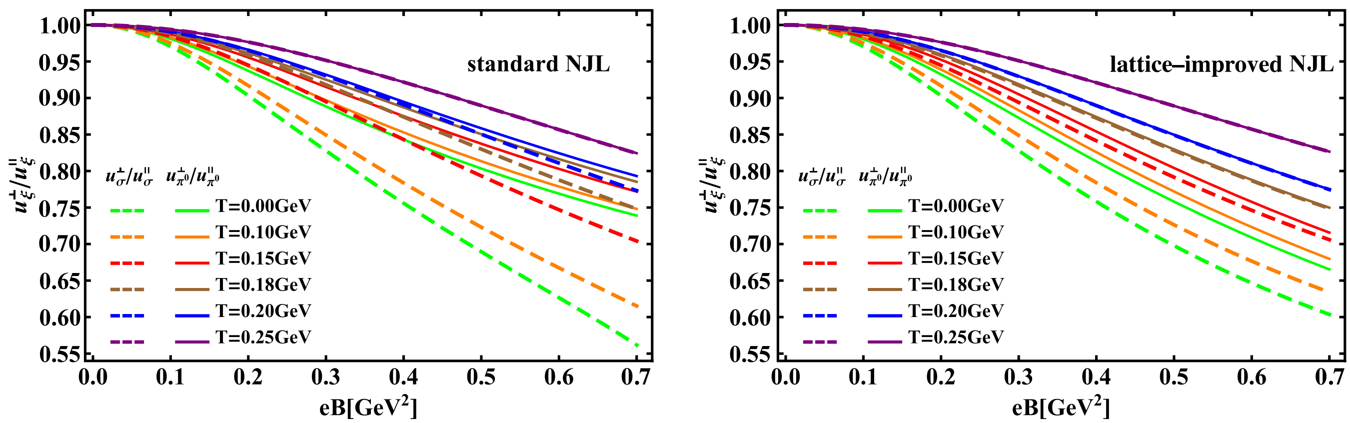

FIG. 16. $u_\xi^\perp/u_\xi^\parallel$ as a function of eB at fixed $T = 0.0$, 0.10, 0.15, 0.18, 0.20, and 0.25 GeV in the standard NJL model (left panel) and the lattice-improved NJL model (right panel), respectively.

In more details, it is shown in Fig. 15 that, at fixed $eB = 0.2$, 0.4, and 0.6 GeV^2, both $u_{\pi^0}^\perp/u_{\pi^0}^\parallel$ and $u_\sigma^\perp/u_\sigma^\parallel$ are temperature independent when $T \lesssim 50$ MeV and then gradually increase to unity as the temperature grows when $T \gtrsim 50$ MeV. Obviously, it agrees with the result in Ref. [75] that $u_\xi^\perp/u_\xi^\parallel$ depends on the magnetic field strength only at low temperatures, where the screening effect of the temperature can be decoupled from that of the magnetic field. But when the temperature becomes sufficiently high, the space symmetry broken by the magnetic field will be recovered by the random thermal motion with the increasing of T [70,75]. Besides, as depicted in Fig. 16, it is found that at low temperatures there is always some discrepancy between $u_{\pi^0}^\perp/u_{\pi^0}^\parallel$ and $u_\sigma^\perp/u_\sigma^\parallel$ (i.e., $u_\sigma^\perp/u_\sigma^\parallel < u_{\pi^0}^\perp/u_{\pi^0}^\parallel < 1$) at finite eB on account of their mass difference, and, when $T \gtrsim T_{\mathrm{pc}}^\parallel$ or $T_{\mathrm{pc}}^\perp$, $u_{\pi^0}^\perp/u_{\pi^0}^\parallel$ and $u_\sigma^\perp/u_\sigma^\parallel$ become degenerate along with the restoration of chiral symmetry.

Finally, we study the eB dependence of the ratio difference $u_{\pi^0}^\perp/u_{\pi^0}^\parallel - u_\sigma^\perp/u_\sigma^\parallel$, which is shown in Fig. 17. And we could find that in the low-temperature region (e.g., $T = 0$, 100, and 150 MeV), when $eB \gtrsim 0.5$ GeV^2, the ratio difference $u_{\pi^0}^\perp/u_{\pi^0}^\parallel - u_\sigma^\perp/u_\sigma^\parallel$ in the standard NJL model continues increasing with eB, while the one in the lattice-improved NJL model reaches saturation, although both of

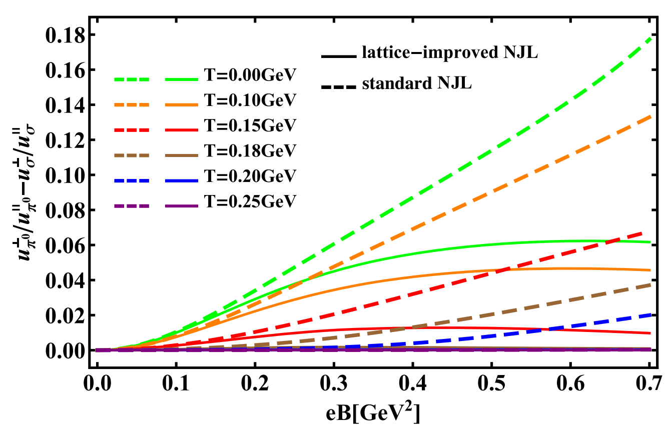

FIG. 17. The ratio difference $u_{\pi^0}^\perp/u_{\pi^0}^\parallel - u_\sigma^\perp/u_\sigma^\parallel$ as a function of eB at fixed $T = 0.0$, 0.10, 0.15, 0.18, 0.20, and 0.25 GeV in the standard NJL model and the lattice-improved NJL model.

them are enlarged with the increase of the magnetic field when $eB < 0.5\ \mathrm{GeV}^2$. Additionally, at a certain eB, $u^{\perp}_{\pi^0}/u^{\parallel}_{\pi^0} - u^{\perp}_{\sigma}/u^{\parallel}_{\sigma}$ in the lattice-improved NJL model is smaller than that in the standard NJL model at low temperatures, which is mainly attributed to the decreasing behavior of $G(eB)$ with respect to eB in the lattice-improved NJL model.

V. SUMMARY AND CONCLUSIONS

In this paper, we incorporate IMC effectively in the lattice-improved two-flavor NJL model by introducing an eB-dependent coupling constant $G(eB)$ to the four-quark interaction [55]. The eB dependence of $G(eB)$ is determined by utilizing the magnetic-field-dependent constituent quark masses inferred from the magnetized baryon mass spectrum which is evaluated in LQCD. The lattice-improved NJL model is shown to exhibit IMC at high temperatures and a reduction of the pseudocritical temperature as the magnetic field grows, which are consistent with the lattice results in Refs. [18,19].

In order to investigate the effects of IMC on the meson screening masses, we analyze the longitudinal and transverse screening masses of neutral pion and sigma meson in terms of the lattice-improved NJL model. For comparison, we also calculate meson screening masses in the standard NJL model that the coupling constant is fixed at $G(eB=0)$. For the sake of the decreasing behavior of the coupling constant $G(eB)$ with increasing eB, the monotonicity of $m_{\pi^0,\mathrm{scr},\parallel}$ and $m_{\pi^0,\mathrm{scr},\perp}$ for neutral pions with respect to the magnetic field in the lattice-improved NJL model is different from that in the standard NJL model when the temperature is adequately high, i.e., $T \gtrsim 150$ MeV. Concerning sigma mesons, because of the same reason above, the monotonicity of $m_{\sigma,\mathrm{scr},\parallel}$ with regard to eB in the lattice-improved NJL model also differs from that in the standard NJL model at low temperatures. Meanwhile, although $m_{\sigma,\mathrm{scr},\perp}$ in both the lattice-improved NJL model and the standard NJL model monotonically increases as eB grows in the low-temperature regime, the extent of increase in the lattice-improved NJL model is smaller than that in the standard NJL model.

In particular, it is interesting to find the fact that, when around the transition temperature, the longitudinal and transverse screening mass differences between σ and π^0 mesons, i.e., $\Delta m^{\parallel}_{\sigma,\pi^0}$ and $\Delta m^{\perp}_{\sigma,\pi^0}$, increase with eB in the standard NJL model but decrease with eB in the lattice-improved NJL model, which is consistent with the prediction by the quark condensate. By the aid of these screening mass differences, $T^{\parallel}_{\mathrm{pc}}$ and $T^{\perp}_{\mathrm{pc}}$, as well as $T^{\parallel}_{\chi}$ and $T^{\perp}_{\chi}$, are defined as (pseudo)critical temperatures of the chiral transition. And we find that, in both the standard and the lattice-improved NJL models, the eB dependences of $T^{\parallel}_{\mathrm{pc}}$ and $T^{\perp}_{\mathrm{pc}}$ ($T^{\parallel}_{\chi}$ and $T^{\perp}_{\chi}$) are in good agreement with that of T_{pc} by the quark condensate. Hence, it implies that exploring behaviors of the screening mass differences of chiral partners (e.g., π^0 and σ mesons) may help to uncover the underlying mechanism of IMC. It is expected that our relevant predictions above could be proved or disproved by lattice QCD simulations in the near future (e.g., a very recent paper [124]), so that we can examine validity and reliability of the hypothesis that the magnetic-field-dependent coupling constant in the NJL model gives rise to IMC in a phenomenological manner.

ACKNOWLEDGMENTS

The authors thank Danning Li, Song He, Yong-Liang Ma, and Shinya Matsuzaki for useful discussion. L. Y. acknowledges the kind hospitality of the Department of Physics and Siyuan Laboratory at Jinan University. The work of L. Y. is supported by the National Science Foundation of China under Grants No. 11605072 and No. 12047569 and the Seeds Funding of Jilin University. X. W. is supported by the start-up funding No. 4111190010 of Jiangsu University.

[1] D. E. Kharzeev, Topology, magnetic field, and strongly interacting matter, Annu. Rev. Nucl. Part. Sci. **65**, 193 (2015).
[2] V. A. Miransky and I. A. Shovkovy, Quantum field theory in a magnetic field: From quantum chromodynamics to graphene and Dirac semimetals, Phys. Rep. **576**, 1 (2015).
[3] J. O. Andersen, W. R. Naylor, and A. Tranberg, Phase diagram of QCD in a magnetic field: A review, Rev. Mod. Phys. **88**, 025001 (2016).
[4] T. Vachaspati, Magnetic fields from cosmological phase transitions, Phys. Lett. B **265**, 258 (1991).
[5] K. Enqvist and P. Olesen, On primordial magnetic fields of electroweak origin, Phys. Lett. B **319**, 178 (1993).
[6] R. C. Duncan and C. Thompson, Formation of very strongly magnetized neutron stars—implications for gamma-ray bursts, Astrophys. J. Lett. **392**, L9 (1992).
[7] V. Skokov, A. Y. Illarionov, and V. Toneev, Estimate of the magnetic field strength in heavy-ion collisions, Int. J. Mod. Phys. A **24**, 5925 (2009).
[8] V. Voronyuk, V. D. Toneev, W. Cassing, E. L. Bratkovskaya, V. P. Konchakovski, and S. A. Voloshin,

(Electro-)Magnetic field evolution in relativistic heavy-ion collisions, Phys. Rev. C **83**, 054911 (2011).

[9] A. Bzdak and V. Skokov, Event-by-event fluctuations of magnetic and electric fields in heavy ion collisions, Phys. Lett. B **710**, 171 (2012).

[10] W.-T. Deng and X.-G. Huang, Event-by-event generation of electromagnetic fields in heavy-ion collisions, Phys. Rev. C **85**, 044907 (2012).

[11] D. Kharzeev and A. Zhitnitsky, Charge separation induced by P-odd bubbles in QCD matter, Nucl. Phys. **A797**, 67 (2007).

[12] V. Okorokov, Estimation of P-odd correlators in heavy ion collisions at RHIC energies 62.4-GeV–200-GeV, arXiv:0908.2522.

[13] K. Fukushima, D. E. Kharzeev, and H. J. Warringa, The chiral magnetic effect, Phys. Rev. D **78**, 074033 (2008).

[14] S. Klevansky and R. H. Lemmer, Chiral symmetry restoration in the Nambu-Jona-Lasinio model with a constant electromagnetic field, Phys. Rev. D **39**, 3478 (1989).

[15] K. Klimenko, Three-dimensional Gross-Neveu model in an external magnetic field, Theor. Math. Phys. **89**, 1161 (1991).

[16] V. Gusynin, V. Miransky, and I. Shovkovy, Dimensional reduction and catalysis of dynamical symmetry breaking by a magnetic field, Nucl. Phys. **B462**, 249 (1996).

[17] I. A. Shovkovy, Magnetic catalysis: A review, Lect. Notes Phys. **871**, 13 (2013).

[18] G. Bali, F. Bruckmann, G. Endrodi, Z. Fodor, S. Katz, S. Krieg, A. Schafer, and K. Szabo, The QCD phase diagram for external magnetic fields, J. High Energy Phys. 02 (2012) 044.

[19] G. Bali, F. Bruckmann, G. Endrodi, Z. Fodor, S. Katz, and A. Schafer, QCD quark condensate in external magnetic fields, Phys. Rev. D **86**, 071502 (2012).

[20] M. Chernodub, Superconductivity of QCD vacuum in strong magnetic field, Phys. Rev. D **82**, 085011 (2010).

[21] M. Chernodub, Spontaneous Electromagnetic Superconductivity of Vacuum in Strong Magnetic Field: Evidence from the Nambu–Jona-Lasinio Model, Phys. Rev. Lett. **106**, 142003 (2011).

[22] R. D. Pisarski and F. Wilczek, Remarks on the chiral phase transition in chromodynamics, Phys. Rev. D **29**, 338 (1984).

[23] S. Borsanyi, Z. Fodor, C. Hoelbling, S. D. Katz, S. Krieg, C. Ratti, and K. K. Szabo (Wuppertal-Budapest Collaboration), Is there still any T_c mystery in lattice QCD? Results with physical masses in the continuum limit III, J. High Energy Phys. 09 (2010) 073.

[24] P. V. Buividovich, M. N. Chernodub, E. V. Luschevskaya, and M. I. Polikarpov, Numerical study of chiral symmetry breaking in non-Abelian gauge theory with background magnetic field, Phys. Lett. B **682**, 484 (2010).

[25] V. V. Braguta, P. V. Buividovich, T. Kalaydzhyan, S. V. Kuznetsov, and M. I. Polikarpov, The chiral magnetic effect and chiral symmetry breaking in SU(3) quenched lattice gauge theory, Phys. At. Nucl. **75**, 488 (2012).

[26] M. D'Elia, S. Mukherjee, and F. Sanfilippo, QCD phase transition in a strong magnetic background, Phys. Rev. D **82**, 051501 (2010).

[27] M. D'Elia and F. Negro, Chiral properties of strong interactions in a magnetic background, Phys. Rev. D **83**, 114028 (2011).

[28] E. M. Ilgenfritz, M. Kalinowski, M. Muller-Preussker, B. Petersson, and A. Schreiber, Two-color QCD with staggered fermions at finite temperature under the influence of a magnetic field, Phys. Rev. D **85**, 114504 (2012).

[29] I. A. Shushpanov and A. V. Smilga, Quark condensate in a magnetic field, Phys. Lett. B **402**, 351 (1997).

[30] N. O. Agasian and I. A. Shushpanov, The Quark and gluon condensates and low-energy QCD theorems in a magnetic field, Phys. Lett. B **472**, 143 (2000).

[31] J. Alexandre, K. Farakos, and G. Koutsoumbas, Magnetic catalysis in QED(3) at finite temperature: Beyond the constant mass approximation, Phys. Rev. D **63**, 065015 (2001).

[32] N. O. Agasian, Chiral thermodynamics in a magnetic field, Phys. At. Nucl. **64**, 554 (2001).

[33] T. D. Cohen, D. A. McGady, and E. S. Werbos, The Chiral condensate in a constant electromagnetic field, Phys. Rev. C **76**, 055201 (2007).

[34] R. Gatto and M. Ruggieri, Dressed Polyakov loop and phase diagram of hot quark matter under magnetic field, Phys. Rev. D **82**, 054027 (2010).

[35] R. Gatto and M. Ruggieri, Deconfinement and chiral symmetry restoration in a strong magnetic background, Phys. Rev. D **83**, 034016 (2011).

[36] A. J. Mizher, M. N. Chernodub, and E. S. Fraga, Phase diagram of hot QCD in an external magnetic field: Possible splitting of deconfinement and chiral transitions, Phys. Rev. D **82**, 105016 (2010).

[37] K. Kashiwa, Entanglement between chiral and deconfinement transitions under strong uniform magnetic background field, Phys. Rev. D **83**, 117901 (2011).

[38] S. S. Avancini, D. P. Menezes, M. B. Pinto, and C. Providencia, The QCD critical end point under strong magnetic fields, Phys. Rev. D **85**, 091901 (2012).

[39] J. O. Andersen, Thermal pions in a magnetic background, Phys. Rev. D **86**, 025020 (2012).

[40] D. D. Scherer and H. Gies, Renormalization group study of magnetic catalysis in the 3d Gross-Neveu model, Phys. Rev. B **85**, 195417 (2012).

[41] K. Fukushima and Y. Hidaka, Magnetic Catalysis Versus Magnetic Inhibition, Phys. Rev. Lett. **110**, 031601 (2013).

[42] T. Kojo and N. Su, The quark mass gap in a magnetic field, Phys. Lett. B **720**, 192 (2013).

[43] F. Bruckmann, G. Endrodi, and T. G. Kovacs, Inverse magnetic catalysis and the Polyakov loop, J. High Energy Phys. 04 (2013) 112.

[44] J. Chao, P. Chu, and M. Huang, Inverse magnetic catalysis induced by sphalerons, Phys. Rev. D **88**, 054009 (2013).

[45] E. S. Fraga, B. W. Mintz, and J. Schaffner-Bielich, A search for inverse magnetic catalysis in thermal quark-meson models, Phys. Lett. B **731**, 154 (2014).

[46] M. Ferreira, P. Costa, O. Lourenço, T. Frederico, and C. Providência, Inverse magnetic catalysis in the $(2+1)$-flavor Nambu-Jona-Lasinio and Polyakov-Nambu-Jona-Lasinio models, Phys. Rev. D **89**, 116011 (2014).

[47] R. L. S. Farias, K. P. Gomes, G. I. Krein, and M. B. Pinto, Importance of asymptotic freedom for the pseudocritical

temperature in magnetized quark matter, Phys. Rev. C **90**, 025203 (2014).

[48] L. Yu, H. Liu, and M. Huang, Spontaneous generation of local *CP* violation and inverse magnetic catalysis, Phys. Rev. D **90**, 074009 (2014).

[49] J. O. Andersen, W. R. Naylor, and A. Tranberg, Inverse magnetic catalysis and regularization in the quark-meson model, J. High Energy Phys. 02 (2015) 042.

[50] E. J. Ferrer, V. de la Incera, and X. J. Wen, Quark antiscreening at strong magnetic field and inverse magnetic catalysis, Phys. Rev. D **91**, 054006 (2015).

[51] C. Providência, M. Ferreira, and P. Costa, Inverse magnetic catalysis in the Polyakov-Nambu-Jona-Lasinio and entangled Polyakov-Nambu-Jona-Lasinio models, Acta Phys. Pol. B Proc. Suppl. **8**, 207 (2015).

[52] R. L. S. Farias, V. S. Timoteo, S. S. Avancini, M. B. Pinto, and G. Krein, Thermo-magnetic effects in quark matter: Nambu–Jona-Lasinio model constrained by lattice QCD, Eur. Phys. J. A **53**, 101 (2017).

[53] S. Mao, Inverse magnetic catalysis in Nambu–Jona-Lasinio model beyond mean field, Phys. Lett. B **758**, 195 (2016).

[54] K. A. Mamo, Inverse magnetic catalysis in holographic models of QCD, J. High Energy Phys. 05 (2015) 121.

[55] G. Endrődi and G. Markó, Magnetized baryons and the QCD phase diagram: NJL model meets the lattice, J. High Energy Phys. 08 (2019) 036.

[56] G. Endrodi, M. Giordano, S. D. Katz, T. G. Kovács, and F. Pittler, Magnetic catalysis and inverse catalysis for heavy pions, J. High Energy Phys. 07 (2019) 007.

[57] A. Tomiya, H.-T. Ding, X.-D. Wang, Y. Zhang, S. Mukherjee, and C. Schmidt, Phase structure of three flavor QCD in external magnetic fields using HISQ fermions, Proc. Sci., LATTICE2018 (**2019**) 163 [arXiv:1904.01276].

[58] S. He, Y. Yang, and P.-H. Yuan, Analytic study of magnetic catalysis in holographic QCD, arXiv:2004.01965.

[59] J. O. Andersen, Chiral perturbation theory in a magnetic background—finite-temperature effects, J. High Energy Phys. 10 (2012) 005.

[60] A. Ayala, R. L. Farias, S. Hernández-Ortiz, L. Hernández, D. M. Paret, and R. Zamora, Magnetic field-dependence of the neutral pion mass in the linear sigma model coupled to quarks: The weak field case, Phys. Rev. D **98**, 114008 (2018).

[61] A. Das and N. Haque, Neutral pion mass in the linear sigma model coupled to quarks at arbitrary magnetic field, Phys. Rev. D **101**, 074033 (2020).

[62] A. Ayala, J. L. Hernández, L. A. Hernández, R. L. S. Farias, and R. Zamora, Magnetic field dependence of the neutral pion mass in the linear sigma model with quarks: The strong field case, Phys. Rev. D **103**, 054038 (2021).

[63] S. Klevansky, J. Janicke, and R. H. Lemmer, Collective modes of the Nambu-Jona-Lasinio model with an external U(1) gauge field, Phys. Rev. D **43**, 3040 (1991).

[64] S. Fayazbakhsh, S. Sadeghian, and N. Sadooghi, Properties of neutral mesons in a hot and magnetized quark matter, Phys. Rev. D **86**, 085042 (2012).

[65] S. Fayazbakhsh and N. Sadooghi, Weak decay constant of neutral pions in a hot and magnetized quark matter, Phys. Rev. D **88**, 065030 (2013).

[66] S. S. Avancini, W. R. Tavares, and M. B. Pinto, Properties of magnetized neutral mesons within a full RPA evaluation, Phys. Rev. D **93**, 014010 (2016).

[67] S. S. Avancini, R. L. S. Farias, M. B. Pinto, W. R. Tavares, and V. S. Timóteo, π_0 pole mass calculation in a strong magnetic field and lattice constraints, Phys. Lett. B **767**, 247 (2017).

[68] S. Mao and Y. Wang, Effect of discrete quark momenta on the Goldstone mode in a magnetic field, Phys. Rev. D **96**, 034004 (2017).

[69] D. G. Dumm, M. I. Villafañe, and N. Scoccola, Neutral meson properties under an external magnetic field in nonlocal chiral quark models, Phys. Rev. D **97**, 034025 (2018).

[70] Z. Wang and P. Zhuang, Meson properties in magnetized quark matter, Phys. Rev. D **97**, 034026 (2018).

[71] H. Liu, X. Wang, L. Yu, and M. Huang, Neutral and charged scalar mesons, pseudoscalar mesons, and diquarks in magnetic fields, Phys. Rev. D **97**, 076008 (2018).

[72] S. S. Avancini, R. L. Farias, and W. R. Tavares, Neutral meson properties in hot and magnetized quark matter: a new magnetic field independent regularization scheme applied to NJL-type model, Phys. Rev. D **99**, 056009 (2019).

[73] N. Chaudhuri, S. Ghosh, S. Sarkar, and P. Roy, Effect of the anomalous magnetic moment of quarks on the phase structure and mesonic properties in the NJL model, Phys. Rev. D **99**, 116025 (2019).

[74] M. Coppola, D. G. Dumm, S. Noguera, and N. Scoccola, Neutral and charged pion properties under strong magnetic fields in the NJL model, Phys. Rev. D **100**, 054014 (2019).

[75] B. Sheng, Y. Wang, X. Wang, and L. Yu, Pole and screening masses of neutral pions in a hot and magnetized medium: A comprehensive study in the Nambu–Jona-Lasinio model, Phys. Rev. D **103**, 094001 (2021).

[76] J. Li, G. Cao, and L. He, Gauge independence of pion masses in a magnetic field within the Nambu–Jona-Lasinio model, Phys. Rev. D **104**, 074026 (2021).

[77] K. Xu, J. Chao, and M. Huang, Effect of the anomalous magnetic moment of quarks on magnetized QCD matter and meson spectra, Phys. Rev. D **103**, 076015 (2021).

[78] V. D. Orlovsky and Y. A. Simonov, Nambu-Goldstone mesons in strong magnetic field, J. High Energy Phys. 09 (2013) 136.

[79] Y. A. Simonov, Pion decay constants in a strong magnetic field, Phys. At. Nucl. **79**, 455 (2016).

[80] T. Kojo, Neutral and charged mesons in magnetic fields: A resonance gas in a non-relativistic quark model, Eur. Phys. J. A **57**, 317 (2021).

[81] Y. Hidaka and A. Yamamoto, Charged vector mesons in a strong magnetic field, Phys. Rev. D **87**, 094502 (2013).

[82] O. Larina, E. Luschevskaya, O. Kochetkov, and O. V. Teryaev, ρ mesons in strong abelian magnetic field in SU(3) lattice gauge theory, Proc. Sci., LATTICE2014 (**2014**) 120 [arXiv:1411.0730].

[83] E. V. Luschevskaya, O. E. Solovjeva, O. A. Kochetkov, and O. V. Teryaev, Magnetic polarizabilities of light

mesons in $SU(3)$ lattice gauge theory, Nucl. Phys. **B898**, 627 (2015).

[84] E. V. Luschevskaya, O. A. Kochetkov, O. V. Teryaev, and O. E. Solovjeva, $\pi^{\pm}$ and $\rho^{0,\pm}$ mesons in a strong magnetic field on the lattice, JETP Lett. **101**, 674 (2015).

[85] E. V. Luschevskaya, O. E. Solovjeva, and O. V. Teryaev, Magnetic polarizability of pion, Phys. Lett. B **761**, 393 (2016).

[86] B. B. Brandt, G. Bali, G. Endrödi, and B. Glässle, QCD spectroscopy and quark mass renormalisation in external magnetic fields with Wilson fermions, Proc. Sci., LATTICE2015 (**2016**) 265 [arXiv:1510.03899].

[87] G. S. Bali, B. B. Brandt, G. Endrődi, and B. Gläßle, Meson masses in electromagnetic fields with Wilson fermions, Phys. Rev. D **97**, 034505 (2018).

[88] H.-T. Ding, S.-T. Li, S. Mukherjee, A. Tomiya, and X.-D. Wang, Meson masses in external magnetic fields with HISQ fermions, Proc. Sci., LATTICE2019 (**2020**) 250 [arXiv:2001.05322].

[89] H.-T. Ding, S.-T. Li, A. Tomiya, X.-D. Wang, and Y. Zhang, Chiral properties of $(2+1)$-flavor QCD in strong magnetic fields at zero temperature, Phys. Rev. D **104**, 014505 (2021).

[90] N. Callebaut, D. Dudal, and H. Verschelde, Holographic study of rho meson mass in an external magnetic field: Paving the road towards a magnetically induced superconducting QCD vacuum?, Proc. Sci., FACESQCD2010 (**2010**) 046 [arXiv:1102.3103].

[91] M. Ammon, J. Erdmenger, P. Kerner, and M. Strydom, Black hole instability induced by a magnetic field, Phys. Lett. B **706**, 94 (2011).

[92] R.-G. Cai, S. He, L. Li, and L.-F. Li, A holographic study on vector condensate induced by a magnetic field, J. High Energy Phys. 12 (2013) 036.

[93] M. Frasca, ρ condensation and physical parameters, J. High Energy Phys. 11 (2013) 099.

[94] M. A. Andreichikov, B. O. Kerbikov, V. D. Orlovsky, and Y. A. Simonov, Meson spectrum in strong magnetic fields, Phys. Rev. D **87**, 094029 (2013).

[95] H. Liu, L. Yu, and M. Huang, Charged and neutral vector ρ mesons in a magnetic field, Phys. Rev. D **91**, 014017 (2015).

[96] H. Liu, L. Yu, and M. Huang, Survival of charged rho condensation at high temperature and density, Chin. Phys. C **40**, 023102 (2016).

[97] H. Liu, L. Yu, M. Chernodub, and M. Huang, Possible formation of high temperature superconductor at an early stage of heavy-ion collisions, Phys. Rev. D **94**, 113006 (2016).

[98] M. Kawaguchi and S. Matsuzaki, Vector meson masses from a hidden local symmetry in a constant magnetic field, Phys. Rev. D **93**, 125027 (2016).

[99] R. Zhang, W.-J. Fu, and Y.-X. Liu, Properties of mesons in a strong magnetic field, Eur. Phys. J. C **76**, 307 (2016).

[100] S. Ghosh, A. Mukherjee, M. Mandal, S. Sarkar, and P. Roy, Spectral properties of ρ meson in a magnetic field, Phys. Rev. D **94**, 094043 (2016).

[101] S. Ghosh, A. Mukherjee, M. Mandal, S. Sarkar, and P. Roy, Thermal effects on ρ meson properties in an external magnetic field, Phys. Rev. D **96**, 116020 (2017).

[102] T. Kunihiro, Chiral restoration, flavor symmetry and the axial anomaly at finite temperature in an effective theory, Nucl. Phys. **B351**, 593 (1991).

[103] W. Florkowski and B. L. Friman, Screening of the meson fields in the Nambu-Jona-Lasinio model, Acta Phys. Pol. B **25**, 49 (1994).

[104] M. Ishii, T. Sasaki, K. Kashiwa, H. Kouno, and M. Yahiro, Effective model approach to meson screening masses at finite temperature, Phys. Rev. D **89**, 071901 (2014).

[105] K.-L. Wang, Y.-X. Liu, L. Chang, C. D. Roberts, and S. M. Schmidt, Baryon and meson screening masses, Phys. Rev. D **87**, 074038 (2013).

[106] M. Ishii, K. Yonemura, J. Takahashi, H. Kouno, and M. Yahiro, Determination of $U(1)_{\mathrm{A}}$ restoration from pion and a_0-meson screening masses: Toward the chiral regime, Phys. Rev. D **93**, 016002 (2016).

[107] X. Cao, S. Qiu, H. Liu, and D. Li, Thermal properties of light mesons from holography, J. High Energy Phys. 08 (2021) 005.

[108] M. Cheng *et al.*, Meson screening masses from lattice QCD with two light and the strange quark, Eur. Phys. J. C **71**, 1564 (2011).

[109] Y. Maezawa, A. Bazavov, F. Karsch, P. Petreczky, and S. Mukherjee, Meson screening masses at finite temperature with Highly Improved Staggered Quarks, Proc. Sci., LATTICE2013 (**2014**) 149 [arXiv:1312.4375].

[110] O. Kaczmarek, E. Laermann, and M. Müller, The thermodynamic and the continuum limit of meson screening masses, Proc. Sci., LATTICE2013 (**2014**) 150 [arXiv:1311.3889].

[111] A. Bazavov *et al.*, Meson screening masses in $(2+1)$-flavor QCD, Phys. Rev. D **100**, 094510 (2019).

[112] D. Ebert, T. Feldmann, and H. Reinhardt, Extended NJL model for light and heavy mesons without q—anti-q thresholds, Phys. Lett. B **388**, 154 (1996).

[113] S. S. Avancini, R. L. S. Farias, M. B. Pinto, T. E. Restrepo, and W. R. Tavares, Regularizing thermo and magnetic contributions within nonrenormalizable theories, Phys. Rev. D **103**, 056009 (2021).

[114] W. R. Tavares, R. L. S. Farias, S. S. Avancini, V. S. Timóteo, M. B. Pinto, and G. A. Krein, Nambu–Jona-Lasinio $SU(3)$ model constrained by lattice QCD: thermomagnetic effects in the magnetization, Eur. Phys. J. A **57**, 278 (2021).

[115] Y. Nambu and G. Jona-Lasinio, Dynamical model of elementary particles based on an analogy with superconductivity. I, Phys. Rev. **122**, 345 (1961).

[116] Y. Nambu and G. Jona-Lasinio, Dynamical model of elementary particles based on an analogy with superconductivity. II, Phys. Rev. **124**, 246 (1961).

[117] S. P. Klevansky, The Nambu–Jona-Lasinio model of quantum chromodynamics, Rev. Mod. Phys. **64**, 649 (1992).

[118] W. Florkowski, Description of hot compressed hadronic matter based on an effective chiral Lagrangian, Acta Phys. Pol. B **28**, 2079 (1997).

[119] J. Schwinger, On gauge invariance and vacuum polarization, Phys. Rev. **82**, 664 (1951).

[120] I. Gradshteyn and I. Ryzhik, *Table of Integrals, Series, and Products*, 7th ed. (Academic Press, New York, 2007).

[121] G. Hellstern, R. Alkofer, and H. Reinhardt, Diquark confinement in an extended NJL model, Nucl. Phys. **A625**, 697 (1997).

[122] W. Bentz and A. W. Thomas, The stability of nuclear matter in the Nambu-Jona-Lasinio model, Nucl. Phys. **A696**, 138 (2001).

[123] J. I. Kapusta andC. Gale, *Finite-Temperature Field Theory: Principles and Applications*, 2nd ed., Cambridge Monographs on Mathematical Physics (Cambridge University Press, Cambridge, England, 2006).

[124] H. T. Ding, S. T. Li, J. H. Liu, and X. D. Wang, Chiral condensates and screening masses of neutral pseudoscalar mesons in thermomagnetic QCD medium, arXiv:2201.02349.